

The allergen Der p3 from house dust mite stimulates store-operated Ca^{2+} channels and mast cell migration through PAR4 receptors

Yu-Ping Lin¹, Charmaine Nelson¹, Holger Kramer^{1,2} and Anant B. Parekh^{1*}

**¹Department of Physiology, Anatomy and Genetics
Parks Road
Oxford
OX1 3PT
UK**

**²Current address:
MRC London Institute of Medical Sciences
Du Cane Road
London
W12 0NN
UK**

***Lead author and author for correspondence:
Email: anant.parekh@dpag.ox.ac.uk
Tel.: ++44-1865-282174**

The house dust mite is the principal source of perennial aeroallergens in man. How these allergens activate innate and adaptive immunity is unclear and therefore there are no therapies targeting mite allergens. Here we show that house dust mite extract activates store-operated Ca^{2+} channels, a common signalling module in numerous cell types in the lung. Activation of channel pore-forming Orai1 subunits by mite extract requires gating by STIM1 proteins. Although mite extract stimulates both PAR2 and PAR4 receptors, Ca^{2+} influx is more tightly coupled to the PAR4 pathway. We identify a major role for the serine protease allergen Der p3 in stimulating Orai1 channels and show that a therapy involving sub-maximal inhibition of both Der p3 and Orai1 channels suppresses mast cell activation to house dust mite. Our results reveal Der p3 as an important aeroallergen that activates Ca^{2+} channels and suggest a therapeutic strategy for treating mite-induced asthma.

Introduction

Allergies have reached epidemic proportions in the western world, with almost one in three people predicted to suffer from an allergy at some point in the individual's lifetime. Although many allergies that develop early in life are not life-threatening themselves, they eventually lead via a process dubbed the 'atopic march' to more serious conditions such as asthma, which can have fatal consequences(Spergel and Paller, 2003). Asthma is a chronic disease of the airways and is estimated to affect more than 300 million people worldwide(Pawankar, 2014).

In the clinic, asthma presents with a range of phenotypes indicating it is a heterogeneous disease(Holgate, 2013). Consistent with this, asthma in an increasing cohort of patients is poorly controlled by the current therapeutic arsenal of β_2 agonist bronchodilators, anti-leukotrienes, inhaled corticosteroids and the anti-IgE antibody omalizumab which are prescribed in varying combinations to manage the disease (Anandan et al., 2010). Evidently, a radical new approach is needed to combat asthma.

One strategy is to target risk factors that are associated with the development of asthma. These factors include genetic predisposition and environmental influences such as exposure to air-borne pollutants and inhaled allergens, particularly those derived from the pyroglyphid house dust mite(Von Mutius, 2009). The house dust mite is a principal source of perennial allergen in man(Platts-Mills et al., 1997). Perennial sensitization to mite allergens in the first three years of life is associated with the symptoms of chronic asthma in older children(Illi et al., 2006). The European Community Respiratory Health Survey I has reported a prevalence for asthma with house dust mite sensitization as high as 21%, although there was significant geographic variation between member states(Bousquet et al., 2007) and a study of Latino women in the USA revealed a prevalence of sensitization to house dust mite of 34-37%(Chew et al., 2009). The two most common types of domestic mite are *Dermatophagoides Pteronyssinus* and *Dermatophagoides Farinae*, which predominate in North America and Europe, respectively. The primary allergens in *Dermatophagoides Pteronyssinus* are the Der p proteins, many of which are proteases (Gregory and Lloyd, 2011).

Allergens from house dust mite stimulate multiple cell types in the lung to release various interleukins and eotaxins that help orchestrate the subsequent inflammatory response (Gregory and Lloyd, 2011; Hammad and Lambrecht, 2015). Interventions that impair the ability of mite allergens to activate the immune system should therefore be of significant therapeutic benefit. One way to accomplish this would be to reduce indoor exposure to mite allergens. This approach has spawned a lucrative domestic mite-removal industry but a meta-analysis of randomized studies found no beneficial effect of these manoeuvres on asthma (Gøtzsche et al., 2004).

An alternative strategy is to understand how house dust mite-derived allergens activate immune cells and the airway remodelling process that is characteristic of chronic asthma, as this will better inform focussed drug design for more effective treatments. A recent study has reported that allergens in extract from dust mite and cockroach evoke cytosolic Ca^{2+} signals in an airway epithelial cell line (Jairaman et al., 2016), but which allergens are required and the underlying signaling pathways are unknown. Here, we show that house dust mite activates Ca^{2+} channels in different cell types that are all involved in the pathogenesis of asthma, and mite-induced Ca^{2+} entry stimulates mast cell migration. We have discovered that the serine protease Der p3 is the key protein amongst the salmagundi of mite allergens that activates the channels and does so through PAR4 receptors. Our results provide mechanistic insight into how allergens activate target cells and identify Der p3 as a target for managing allergic asthma.

Results

House dust mite extract activates Ca^{2+} signals in various cell types associated with asthma

We focussed on allergens derived from *Dermatophagoides Pteronyssinus*, as this mite has a broad geographic distribution. To separate Ca^{2+} release from internal stores and Ca^{2+} influx, mite whole body extract was applied to cells bathed initially in Ca^{2+} -free external solution. External Ca^{2+} was then readmitted a few minutes later to measure Ca^{2+} entry. Mite extract triggered Ca^{2+} release from human mast cells surgically removed from patients with nasal polyposis and this was followed by prominent Ca^{2+} entry (Figure 1A). Ca^{2+} signals to mite extract in these cells were similar to the biphasic response evoked by the SERCA pump inhibitor thapsigargin and which comprises Ca^{2+} release from the stores followed by Ca^{2+} influx through store-operated Ca^{2+} release-activated Ca^{2+} (CRAC) channels in the plasma membrane (Figure 1A). Ca^{2+} signals were evoked when extract was applied to RBL-2H3 mast cells (Figure 1B). Both Ca^{2+} release and the rate and extent of Ca^{2+} influx increased with the dose of extract applied (Figure 1B). The rate of Ca^{2+} entry induced by a high dose of mite extract was a little slower than that evoked by a maximally effective concentration of thapsigargin (Figure 1C). Bone marrow-derived mouse mast cells also responded to house dust mite extract (Figure 1F). Mite extract triggered small but prolonged Ca^{2+} release from human bronchial epithelial cells and this was followed by prominent Ca^{2+} entry (Figure 1D). Both human embryonic kidney (HEK-293) cells (Figure 1E) and human jurkat T lymphocytes (Figure 1F)

responded to mite extract in a manner qualitatively similar to mast and epithelial cells. Very little Ca^{2+} entry occurred following readmission of external Ca^{2+} to the various cell types perfused with Ca^{2+} -free solution for the same time but in the absence of mite extract (labeled background in Figures 1D and 1E). We noticed that the kinetics of Ca^{2+} release to mite extract varied markedly between different cell types. These differences are due to the activation of different cell-surface receptors and will be addressed in more detail in a later section describing the involvement of PAR receptors.

Potential problems with studies on house dust mite extract relate to reported differences in efficacy between commercial suppliers as well as variations between batches from a given supplier. To mitigate against the former, we used one supplier (Greer) throughout our study. We also tested each batch of extract we received for consistency by applying the same dose (400 $\mu\text{g}/\text{ml}$). Generally, reliability between batches was good (Supplemental Figure 1).

Although house dust mite extract has been used in several studies involving fluorescence measurements of cytosolic Ca^{2+} , we checked to see whether it exhibited any intrinsic fluorescence. Mite extract was only weakly fluorescent over the wavelengths we have used and this did not impact qualitatively or quantitatively on our data (Supplemental Figure 1).

House dust mite extract stimulates Ca^{2+} release from InsP_3 -sensitive stores followed by Ca^{2+} entry through store-operated CRAC channels.

Agonists generally release Ca^{2+} from the endoplasmic reticulum (ER) via the second messenger inositol 1,4,5-trisphosphate (InsP_3), produced following activation of phospholipase C. Inhibition of phospholipase C with U73122 abolished Ca^{2+} release evoked by mite extract (Figure 1G), suggesting the Ca^{2+} release phase was dependent on InsP_3 production. Consistent with this, expression of a cytosolic InsP_3 buffer reduced the rate of Ca^{2+} release to mite extract (Figure 1H). Following exposure to thapsigargin in Ca^{2+} -free solution to deplete the Ca^{2+} stores, stimulation with mite extract failed to raise cytosolic Ca^{2+} (Figure 1I). Collectively, these results demonstrate that house dust mite extract releases Ca^{2+} from the InsP_3 - and thapsigargin-sensitive ER.

We compared the pharmacological profile of the Ca^{2+} influx pathway activated by mite extract with that of the CRAC channel. Ca^{2+} entry through CRAC channels in RBL-2H3 cells was evoked by depleting stores with thapsigargin (Figure 2A). Structurally distinct CRAC channel blockers inhibited thapsigargin-evoked Ca^{2+} influx (Figure 2B) and Ca^{2+} entry to mite extract (Figure 2A, 2C) with very similar pharmacological profiles.

A strong hyperpolarization or fast inhibition of Ca^{2+} clearance pathways by mite extract could translate into a rapid rate of Ca^{2+} entry even though only a few Ca^{2+} channels have been activated. Ba^{2+} permeates CRAC channels but is not extruded from the cytosol by Ca^{2+} ATPase pumps. Ba^{2+} also binds to fura 2, albeit with ~ 3 -fold lower affinity than Ca^{2+} . Therefore the rate of rise of cytosolic Ba^{2+} provides a good estimate of the number of open CRAC channels (Bakowski and Parekh, 2007). Stimulation with mite extract led to a significant increase in the rate of Ba^{2+} entry compared with the background rate, although it was slower than that observed when Ca^{2+} was readmitted instead (Figure 2D). Stimulated Ba^{2+} entry was $66.2 \pm 4.6\%$ of the Ba^{2+} flux seen in response to 2 μM thapsigargin,

consistent with activation of a sizeable number of CRAC channels. To rule out a major contribution from the membrane potential to Ca^{2+} entry induced by mite extract, we clamped the membrane potential close to 0 mV by incubating cells in high (100 mM) K^{+} -containing external solution and increased the concentration gradient for Ca^{2+} entry by raising external Ca^{2+} to 5 mM. Mite extract still evoked robust Ca^{2+} entry (Figure 2E) and this was $80.8 \pm 15\%$ of that induced by thapsigargin under the same conditions.

To test more directly whether mite extract activated CRAC channels, we carried out whole cell patch clamp experiments in RBL-2H3 cells to measure the endogenous CRAC current (I_{CRAC}). Cells were dialyzed with a pipette solution containing Ca^{2+} buffered at 150 nM to prevent passive depletion of stores and bathed in Ca^{2+} -free external solution. In the presence of house dust mite extract, no detectable Ca^{2+} current was detectable until external Ca^{2+} was readmitted (Figure 2F). Now, I_{CRAC} developed rapidly as judged by the steep inward rectification, non-voltage dependent activation and reversal potential $> +70$ mV (Figure 2G). The current-voltage relationship of mite-induced I_{CRAC} was identical to that evoked following dialysis with InsP_3 (Figure 2G). The amplitude of I_{CRAC} in response to mite extract challenge was smaller ($\sim 50\%$) than that induced by store depletion with InsP_3 (Figure 2H). When external Ca^{2+} was readmitted to cells pre-exposed to mite extract and then dialysed with a pipette solution containing a maximally effective concentration of InsP_3 , I_{CRAC} had the same amplitude as that induced by InsP_3 alone (Figure 2H). Hence I_{CRAC} induced by mite extract is not additive with InsP_3 -evoked I_{CRAC} , consistent with activation of the same population of CRAC channels.

House dust mite extract activates PAR2 and PAR4 receptors, but PAR4 couples more strongly to Ca^{2+} entry.

A previous study reported that dust mite and cockroach extract triggered Ca^{2+} signals in airway epithelia through protease activated receptor type 2 (PAR2) (Jairaman et al., 2016), a member of the protease activated receptor family of G protein coupled receptors that stimulate phospholipase C. However, knockdown of PAR2 receptors only partially reduced the cytosolic Ca^{2+} signal (Jairaman et al., 2016), suggesting additional mechanisms are involved.

We found that cytosolic Ca^{2+} signals to mite extract challenge in Ca^{2+} -free solution were often bi-phasic in nature in the various cell types we used. An initial transient Ca^{2+} release event was followed by a slower but more sustained phase. Striking examples of this second phase can be seen in Figures 1B, 1G and 2E. However, the second phase was not always clearly resolvable (Figure 3A; compare grey and black traces). In nasal mast cells, the second phase was clear but the initial transient Ca^{2+} release component was absent (Figure 1A). This was also the case in RBL-2H3 cells with lower doses of mite extract (Figure 1B). Nevertheless in both cases store-operated Ca^{2+} entry was prominent. We analyzed the size of the second phase for each RBL-2H3 cell and found it could be classified into three relative groups: big, medium and small (Figure 3A). Ca^{2+} influx correlated well with the size of the second phase of Ca^{2+} release (Figure 3B) but not with the larger but more transient first phase (Supplemental Figure 2). We therefore analyzed, on a cell by cell basis, the extent of Ca^{2+} mobilization in the first and big second phases by integrating the area

under the curve for each Ca^{2+} release component. In all cells, the integrated Ca^{2+} signal for the second phase was larger than the first (normalized first phase integral was $100 \pm 9\%$ compared with $201 \pm 8\%$ for the second phase, $p < 0.01$).

The bi-phasic pattern of Ca^{2+} release to mite extract suggests a two step process with one pathway activating quickly and the other more slowly. We therefore hypothesized that two different PAR receptor sub-types were involved in the Ca^{2+} signal generated by mite extract. RT-PCR experiments in RBL-2H3 cells (Figure 3C) and HEK-293 cells (Supplemental Figure 2) revealed that multiple protease-activated receptors were indeed co-expressed in these cell types.

Different PARs have distinct properties that lead to different patterns of downstream signalling (French and Hamilton, 2016). PAR1 and PAR2 receptors desensitize rapidly whereas PAR4 receptors do not. PAR2 receptors are weakly activated by thrombin compared with other PAR receptors (Coughlin, 2000). PAR4 receptors have low affinity for thrombin, with an EC_{50} of ~ 5 nM, compared with ~ 0.2 nM for PAR1 and PAR3. We exploited these differences to obtain functional evidence for multiple co-expressed PARs. Application of trypsin, which activates all PAR receptors, evoked Ca^{2+} release followed by Ca^{2+} influx in RBL-2H3 cells (Figure 3D). A second pulse of trypsin failed to elicit Ca^{2+} release, consistent with receptor desensitization (Supplemental Figure 3). Following loss of the trypsin response due to desensitization, mite extract evoked only the second phase of Ca^{2+} release (Figure 3E); the initial transient Ca^{2+} release component was lost (Figure 3E). However, mite-induced store-operated Ca^{2+} entry was unaffected by desensitization of the trypsin response (Figure 3E). To further test for a role for PAR2 receptors in mite-extract driven Ca^{2+} signalling, we pre-treated cells with a PAR2 antagonist. The rapid phase of Ca^{2+} release to mite extract was almost abolished but the second phase was still present and this was followed by prominent Ca^{2+} entry (Figure 3F).

Thrombin evoked strong Ca^{2+} signals in RBL-2H3 and HEK-293 cells, demonstrating the presence of functional protease-activated receptors independent of PAR2 (Figure 3G). Because mite extract still evoked Ca^{2+} signals after trypsin-driven desensitization of PAR1 and PAR2 receptors (Figure 3E), we focused on PAR3 and PAR4 receptors. PAR3 receptors have a considerably higher affinity for thrombin than PAR4. A dose-response curve to thrombin revealed that relatively high concentrations of agonist were required to elicit Ca^{2+} release (inset to Figure 3G; EC_{50} of 110 nM), pointing to a major role for PAR4 receptors. In agreement with this, the PAR4 antagonist ML354 significantly reduced both Ca^{2+} release and subsequent Ca^{2+} entry to thrombin (Figure 3H; rate of Ca^{2+} entry to thrombin in ML354-treated cells was reduced by $65 \pm 3\%$ compared with thrombin alone) but had no effect on either Ca^{2+} release or Ca^{2+} entry following trypsin activation (Figure 3I). ML354 also had no inhibitory effect on thapsigargin-evoked Ca^{2+} signals (Supplemental Figure 3), ruling out direct inhibition of CRAC channels. Pre-treatment with ML354 failed to affect the initial Ca^{2+} release response to house dust mite but the second phase was lost (Figure 3J). Ca^{2+} influx to mite extract was also significantly reduced (Figure 3J; rate of Ca^{2+} entry to mite extract in ML354 was reduced by $92 \pm 6\%$ compared with mite extract alone, after correction for the background Ca^{2+} entry rate).

Collectively, our results demonstrate that mite extract activates two distinct PAR receptors in the same cells, PAR2 and PAR4. PAR2 receptor activation leads to rapid but transient Ca^{2+} release from the stores whereas PAR4 receptors generate a smaller but more prolonged Ca^{2+} mobilization component. This latter phase is more tightly linked to store-operated Ca^{2+} entry. To test this concept more directly, we applied the small peptide agonist AYPGFK-NH2 that is specific to PAR4 receptors (Faruqi et al., 2000). The peptide led to a dose-dependent increase in Ca^{2+} release followed by prominent store-operated Ca^{2+} entry (Figure 3K). The Ca^{2+} release component was abolished by U73122 (Figure 3L). The CRAC channel blocker BTP2 suppressed Ca^{2+} entry activated by the peptide, leaving Ca^{2+} release intact (Figure 3L). A low dose of peptide (8.5 μM) triggered slow, sluggish Ca^{2+} release that was reminiscent of the second phase of Ca^{2+} release induced by mite extract and this was followed by store-operated Ca^{2+} entry (Figure 3K).

PAR4 receptors are cleaved by serine proteases to reveal an N-terminal receptor-activating domain that binds to the tethered ligand binding site on the second extracellular loop to activate the receptor (French and Hamilton, 2016). To see whether mite extract cleaved PAR4 receptors, we challenged cells with the agonist AYPGFK-NH2 to which fluorescein had been conjugated and used FACS to assess agonist binding to the cell membrane. Substantial fluorescence was seen in cells exposed to fluorescein tagged-AYPGFK-NH2 and this was significantly reduced by pre-treatment of cells with house dust mite extract (Figure 3M; see Figure legend for details). Hence mite extract cleaves PAR4 receptors, enabling the endogenous tethered ligand to bind to the ligand binding site and thereby reduce the binding of the fluorescent peptide. In a second approach, we used immunofluorescence to monitor fluorescent agonist association with the cell surface. Fluorescent peptide labeled the cell surface in resting cells. However, after exposure to mite extract, fluorescent labeling was significantly reduced (see also page 13; Supplemental Figure 6).

Ca^{2+} influx to mite extract requires STIM1 gating of Orai1

Functional CRAC channels are composed of two core protein elements: the pore-forming subunit Orai1 and the ER Ca^{2+} sensor STIM1 (reviewed in (Lewis and Prakriya, 2015)). Upon a fall in ER Ca^{2+} content, STIM1 proteins oligomerize and then translocate to junctional ER, located just below the plasma membrane where they bind to and gate the Orai1 channels. STIM1 clusters or puncta are readily visible in light microscopy following overexpression of tagged protein such as STIM1-YFP.

Knockdown of STIM1 reduced protein expression in RBL-2H3 cells by ~60% (Figures 4A and 4B), and significantly decreased Ca^{2+} influx to mite extract (Figures 4C and 4D). Similar results were obtained when Orai1 was knocked down instead (Figures 4A-4D). Jaiaaram et al. reported that STIM1 and Orai1 were necessary for allergen-induced Ca^{2+} entry in airway epithelial cells but it is not known if STIM1 gating of Orai1 is required. We expressed STIM1-YFP and used TIRF microscopy to measure STIM1 puncta just below the plasma membrane. In resting cells, a few punctate-like structures were occasionally visible (Figure 3E, left hand panel). However, after mite exposure, numerous puncta were resolvable (Figure 3E, right hand panel). Similar results were

obtained with confocal microscopy. Few, if any, STIM1-YFP clusters were apparent in confocal images of resting cells (Figure 3F, left hand panel) but clusters formed after exposure to mite extract (Figure 3F, right hand panel), although these were less numerous compared with thapsigargin stimulation (Figure 3F, middle panel).

Overexpression of STIM1 led to a modest but significant increase in the rate of Ca^{2+} influx induced by mite extract, and this was further enhanced by co-expression of recombinant Orai1 (Figure 4G).

To test whether gating of Orai1 by STIM1 was required for mite-induced activation of Ca^{2+} entry, we compared mite-induced Ca^{2+} influx following expression of wild type Orai1 or Orai1 mutants that cannot be gated by STIM1, after knock down of endogenous Orai1. The CRAC-activating domain of STIM1 interacts with a leucine-rich coiled-coil motif on the C terminus of Orai1. Mutation of leucine 273 (L273S) in this region reduces STIM1-Orai1 interaction and CRAC channel activation (Lewis and Prakriya, 2015). Ca^{2+} influx evoked by mite extract was substantially reduced by Orai1 knock down (Figure 4H). Overexpression of wildtype Orai1 rescued Ca^{2+} influx but overexpression of L273S-Orai1 did not (Figure 4H). A short stretch of amino acids on Orai1 ($^{81}\text{LSRAK}^{85}$) is thought to be essential for gating by STIM1. The $^{81}\text{AARAE}^{85}$ -Orai1 mutant showed no Ca^{2+} entry in response to store depletion (Gudlur et al., 2014). Following knockdown of endogenous Orai1, mite-evoked Ca^{2+} influx could not be rescued by co-expression of $^{81}\text{AARAE}^{85}$ -Orai1 and STIM1 (Figure 4H).

Collectively, these results establish that house dust mite-induced Ca^{2+} entry requires STIM1 gating of Orai1 channels and in a manner indistinguishable from conventional gating of Orai1 by store depletion.

Identifying the allergens in house dust mite that activate CRAC channels

Dermatophagoides pteronyssinus extract contains numerous allergens, adjuvants and signalling molecules. We therefore asked whether the component(s) of mite extract that activated CRAC channels was protein or non-protein in nature. We reasoned that protein components should be denatured by boiling and therefore lose activity. To test this, we boiled house dust mite extract at 100°C for 10-15 minutes and then, after cooling it back to room temperature, we applied the extract to fura 2-loaded RBL-2H3 cells. Boiled extract triggered the initial transient phase of Ca^{2+} release but the second sustained phase of Ca^{2+} release and Ca^{2+} influx were suppressed (Figures 5A and 5B). By contrast, robust Ca^{2+} entry was elicited by mite extract that had not been boiled (Figures 5A and 5B).

Several Der p allergens have protease activity. Der p1 is a cysteine protease, whereas Der p3, p6 and p9 are serine proteases. The serine protease inhibitor nafamostat inhibited Ca^{2+} influx by $\sim 80\%$ (Figure 5C). Similar results were obtained with structurally distinct serine protease inhibitors camostat and aprotinin (Figure 5C), although aprotinin was less effective at the concentrations tested. Nafamostat did not affect thapsigargin-evoked Ca^{2+} entry (Supplemental Figure 4), ruling out an action on store-operated Ca^{2+} influx *per se*. The cysteine protease inhibitor E-64 had no inhibitory effect on mite-induced Ca^{2+} entry (Figure 5C).

We asked whether all mite serine proteases were able to activate Ca^{2+} influx or if one enzyme played an inimitable role. To address this, we carried out

fractionation experiments and then tested the ability of each fraction to activate Ca^{2+} entry. Although the various serine proteases are synthesized as inactive pro-enzymes, it is important to note that the pro-moieties have already been cleaved within the mite extract and therefore the various proteases are in their active forms. Typical results are shown in Figure 5D. Fraction A13, for example, caused Ca^{2+} release followed by robust Ca^{2+} entry. Fraction A11 also caused moderate Ca^{2+} release followed by Ca^{2+} influx whereas fraction B04 failed to cause Ca^{2+} release or significant Ca^{2+} entry (the Ca^{2+} signal to B04 was similar to the background trace). We ran each fraction in a coomassie blue gel (Figure 5E) and then identified the Der p proteins present by using mass spectrometry. Fraction A13 contained Der p1, p2, p3, p7 and p8 (Figure 5F). Fraction A11 contained Der p2, p3 and p10 whereas the inactive fraction B04 had no Der p proteins (Figure 5F). All proteins identified by mass spectroscopy are listed in the Supplemental Table 1. The only serine protease that was consistently found in the active fractions but was absent from Der p-containing inactive fractions was Der p3.

Recombinant Der p3 potentiates Ca^{2+} entry to mite extract

Based on the preceding results, we hypothesized that Der p3 was an important mite component that regulated store-operated Ca^{2+} influx. We therefore sought to apply Der p3 to see whether it stimulated Ca^{2+} entry. Similar to other trypsin-like serine proteases, Der p3 is synthesized as the inactive pro-enzyme. We therefore purified pro-Der p3 protein following overexpression in a bacterial expression system by inserting a his-tag upstream of the pro-moiety. His-pro-Der p3 activated Ca^{2+} signals in RBL-2H3 or HEK-293 cells very weakly, suggesting cleavage of the pro-moiety was indeed required for activity (Figure 5H, labelled pro-Der p3). Our attempts at generating Der p3 protein by deleting or bypassing the pro-sequence were thwarted by the fact that constitutive Der p3 serine protease digested the bacteria used for expression. We thus were forced to identify alternative strategies for activating Der p3. Pro-Der p3 is cleaved to active Der p3 by the cysteine protease activity of Der p1 (Dumez et al., 2008). We reasoned that incubation of recombinant his-pro-Der p3 with a low dose of mite extract that itself barely evoked Ca^{2+} influx should result in cleavage of his-pro-Der p3 to Der p3 by Der p1 within the extract, leading to enhanced Ca^{2+} influx. We tested various doses of mite extract to find one that failed to evoke Ca^{2+} influx larger than the background level (the level seen when external Ca^{2+} was readmitted to cells incubated only in Ca^{2+} free solution for the same time). 30-60 $\mu\text{g}/\text{ml}$ of extract triggered modest Ca^{2+} release and little Ca^{2+} entry (Figure 5H, labelled L.D. (low dose) HDM). Cleavage of the his-pro-Der p3 by Der p1 within mite extract should lead to loss of the his tag. Incubation of his-pro-Der p3 with 30 $\mu\text{g}/\text{ml}$ mite extract for 10-20 minutes at 37°C led to loss of the his tag (Figure 5G) and this was prevented by pre-treatment with the cysteine protease inhibitor E-64 (Figure 5G). Therefore incubation of his-pro-Der p3 with mite extract leads to cysteine protease-dependent cleavage of the pro-enzyme. Pre-incubation of his-pro-Der p3 with the low dose of mite extract resulted in robust Ca^{2+} entry (Figure 5H), whereas application of either pro-Der p3 or the low dose of mite extract alone, which had been kept at 37°C for the same time, failed to elicit Ca^{2+} influx (Figure 5H). To show more directly that cleavage of pro-Der p3 was required for Ca^{2+} entry, we mutated several amino acids within the cleavage

site in pro-Der p3. Following incubation of this mutated pro-Der p3 (labelled uncut Der p3) with a low dose of mite extract, Ca^{2+} influx was almost abolished when compared with wild-type pro-Der p3 (Figure 5I).

Addition of E-64 to mite extract for 10 minutes prior to incubation at 37°C with his-tagged pro-Der p3 abolished Ca^{2+} influx (Figure 5J). A further prediction would be that if E-64 was added after mite extract had been pre-incubated with his-tagged pro-Der p3 for 10 minutes, cleavage should already have occurred and so E-64 now should have no inhibitory effect. This was indeed the case; robust Ca^{2+} influx still occurred (Figure 5J). Ca^{2+} influx evoked by a low dose of mite extract incubated with his-tagged pro-Der p3 was suppressed either in cells in which Orai1 had been knocked down (Figure 5J) or in the presence of BTP2 (Supplemental Figure 4), confirming Ca^{2+} entry was mediated by CRAC channels.

Catalytic activity of Der p3 is required for Ca^{2+} influx

We asked whether catalytic activity of Der p3 was required for potentiating Ca^{2+} influx. Pre-treatment of his-tagged pro-Der p3 with nafamostat prior to addition of a low dose of house dust mite extract suppressed Ca^{2+} influx (Figure 6A, trace labelled Nafamostat; L.D. HDM + pro-Der p3), compared with the corresponding control lacking nafamostat (Figure 6A).

Der p3 is a serine protease with trypsin-like activity. The catalytic site of trypsin involves the triad of serine 195, histidine 57 and aspartate 102. Using bioinformatics, we identified corresponding residues in Der p3 as serine 214, histidine 69 and aspartate 114. We mutated either serine 214 or aspartate 114 to alanines in his-tagged pro-Der p3 (S214A-Der p3 and D214A-Der p3, respectively) and then incubated the mutant proteins with a low dose of mite extract. Little Ca^{2+} entry occurred when either D114A-Der p3 or S214A-Der p3 was added to the mite extract instead of Der p3 (Supplemental Figure 4). We then used D114A-Der p3 or S214A-Der p3 as competitive antagonists of Der p3, to see whether each mutant could inhibit Ca^{2+} influx induced by endogenous Der p3 contained within a high dose of house dust mite. Both mutant Der p3 proteins suppressed Ca^{2+} influx to mite extract (Figure 6B). The mutants also suppressed the second slow phase of Ca^{2+} release as well as Ca^{2+} influx, in agreement with these phases reflecting Der p3-dependent cleavage of PAR4 receptors.

Collectively, these results demonstrate that i) the catalytic activity of Der p3 is required for activation of Ca^{2+} entry and ii) catalytically inactive Der p3 can prevent Ca^{2+} influx to house dust mite, suggesting Der p3 in the extract is a key component for Ca^{2+} influx. We considered two possible mechanisms: i) Der p3 was the critical mediator that stimulated Ca^{2+} influx through its serine protease activity or ii) through serine protease activity, Der p3 cleaved a non-serine protease component in the mite extract which then activated Ca^{2+} influx. If the latter mechanism is correct, inhibition of serine protease activity after incubation of a low dose of mite extract with his-tagged pro-Der p3 should not reduce Ca^{2+} influx since Der p3 would have cleaved and thus activated the downstream component within the extract. However, addition of nafamostat after his-tagged pro-Der p3 had been incubated with a low dose of mite extract suppressed Ca^{2+} influx (Figure 6A; trace labelled LD HDM + pro-Der p3; nafamostat), demonstrating that continuous catalytic activity of Der p3 was important for activation of Ca^{2+} entry.

Der p1 and pro-Der p3 are sufficient to evoke Ca^{2+} influx

To address whether Der p1 and Der p3 were sufficient for activation of Ca^{2+} influx, we mixed recombinant commercially available Der p1 (purity shown in silver stained gel in Supplemental Figure 5) with purified his-tagged pro-Der p3 and tested whether the combination activated Ca^{2+} influx. Neither Der p1 nor his-tagged pro-Der p3 alone evoked Ca^{2+} entry above the background (Figure 6C). However, the combination triggered both Ca^{2+} release and Ca^{2+} influx (Figure 6C). BTP2 inhibited the Ca^{2+} entry component (Supplemental Figure 5). Pre-treatment of Der p1 with E-64 prior to addition of his-pro-Der p3 suppressed Ca^{2+} influx (Figure 6C), confirming that the cysteine protease activity of Der p1 was required for activation of Der p3. As expected, very little Ca^{2+} release occurred in E-64, as neither Der p1 nor Der p3 were now active (Figure 6C). Ca^{2+} entry to the combination of Der p1 and pro-Der p3 was blocked by nafamostat (Figure 6C). Ca^{2+} release was also impaired by nafamostat, consistent with a major role for Der p3 in activating PAR receptors. As these proteins were the only two components present in these experiments, the data strongly support the view that Der p3 is acting directly and not through another component within mite extract.

We repeated the above experiments but with commercially available pro-Der p3. Silver staining confirmed the purity of the recombinant protein (Supplemental Figure 5). Whereas a low dose of mite extract was unable to activate Ca^{2+} entry, the addition of commercial pro-Der p3 led to robust Ca^{2+} influx (Figure 6D). Commercial pro-Der p3 alone did not cause resolvable Ca^{2+} influx (Figure 6D). Boiling house dust mite extract abolished store-operated Ca^{2+} influx (Figure 5A). Boiling commercial pro-Der p3 prior to incubation with mite extract also abolished Ca^{2+} entry (Supplemental Figure 4).

Finally, we checked to see whether Der p3 was able to activate PAR4 receptors. Pre-treatment with a low dose of mite extract reduced fluoresecin-conjugated PAR4 peptide binding and this was decreased further by addition of recombinant pro-Der p3 (Supplemental Figure 6). Importantly, addition to the mite extract of S214A-Der p3, which is catalytically inactive, failed to reduce agonist binding (Supplemental Figure 6), demonstrating catalytic activity of Der p3 was required for PAR4 receptor activation. The S214A-Der p3 mutant also prevented the reduction in agonist binding that was seen in response to a low dose of mite extract alone (Supplemental Figure 6). This is consistent with the mutant acting as a competitive antagonist of endogenous Der p3 within the mite extract, in agreement with data shown in Figure 6B and Supplemental Figure 4.

Suppressed serine protease activity of Der p3 mutants

Both Der p1 and pro-Der p3 alone had very little protease activity but the combination was highly active, when measured directly using a colorimetric assay (Supplemental Figure 7). Neither D114A-Der p3 or S214A-Der p3 exhibited activity, and weak activity was seen with the uncut Der p3 mutant (Supplemental Figure 7), demonstrating that the mutant Der p3 proteins all had impaired catalytic inactivity.

The combination of sub-maximal doses of BTP2 and nafamostat prevent Ca^{2+} entry to mite extract

Since mite extract activates CRAC channels through Der p3, we hypothesized that

the combination of partial block of Der p3 with partial block of CRAC channels should suppress the Ca^{2+} entry signal. Sub-maximal concentrations of each inhibitor reduce off-target effects and thus increase the therapeutic window. A combination therapy using low doses of anti-leukotrienes and CRAC channel blockers has proved effective in suppressing activation of mast cells (Di Capite et al., 2009). Ca^{2+} influx induced by mixing a low dose of mite extract with pro-Der p3 was reduced slightly by a sub-maximal dose of nafamostat (Figures 6E and 6F) and more so by the IC_{50} concentration of BTP2 (Figures 6E and 6F). However, the combination of these doses of nafamostat and BTP2 abolished Ca^{2+} influx (Figures 6E and 6F).

Cell migration induced by mite extract involves CRAC channels

Stimulation with mite extract led to marked protrusions of the RBL-2H3 mast cell surface within a few tens of seconds (Figure 7A). Almost all cells responded in this way (Figure 7B). Block of phospholipase C with U73122 suppressed the appearance of protrusions (Figure 7B). Inhibition of CRAC channels with BTP2 or removal of external Ca^{2+} reduced the fraction of cells that responded by generating protrusions (Figure 7B). Treatment with cytochalasin D abolished the formation of protrusions evoked by mite extract (Figure 7B), suggesting that actin is involved in driving the surface extensions. We quantified the size of the protrusions using electron microscopy. Whereas in resting mast cells few protrusions were evident (Figure 7C, upper panel), several protrusions could be observed at the same time after treatment with mite extract (Figure 7C, lower panel). The protrusions were typically 4-12 μm in length and 2-4 μm in diameter. Protrusions of these dimensions are characteristic of migrating cells. Mite extract induced prominent cell migration (Figure 7D) and this was significantly but partially reduced by knockdown of Orai1 or addition of BTP2 (Figure 7E). Addition of S214A-Der p3 inhibited mite extract-induced migration as did block of PAR4 receptors with ML354 (Figure 7E). Migration was suppressed by prior boiling of mite extract (Figure 7E). We also measured responses to mite extract from primary bone marrow-derived mouse mast cells. Mite extract triggered robust store-operated Ca^{2+} entry in these mast cells (Figure 7F), and this was blocked by BTP2 (Figure 7G), by ML354 (Figure 7G), and addition of S214A-der p3 to mite extract (Figure 7G). A significant increase in mast cell migration was observed when bone marrow-derived mast cells were exposed to house dust mite extract (Figure 7H-I), and this was inhibited by BTP2 (Figure 7I).

Discussion

Globally, the house dust mite is the principal source of aeroallergens associated with symptomatic allergic airway diseases in man. Sensitization to mite-derived allergens occurs before sensitization to other environmental allergens, and mite allergens initiate primary events within the immune system that other allergens require. For example, house dust mite is the sensitizing agent to allergic reactions including asthma that occur following mollusc ingestion, including snails and limpets (Azofra and Lombardero, 2003).

Asthma is a complex disease that involves a dynamic interplay between several different cell types within the lung (Hammad and Lambrecht, 2015). A common signalling module in all these cells is store-operated Ca^{2+} entry, which

plays a central role in the synthesis of lipid mediators and in the transcription and secretion of chemokines and cytokines (Parekh, 2010). Mice deficient in either STIM1 (Baba et al., 2008) or Orai1 (Vig et al., 2008) exhibit impaired delayed hypersensitivity and store-operated Ca^{2+} channel blockers reduce the severity of lung dysfunction in animal models of asthma (Sutovska et al., 2016). Several allergens in house dust mite are serine proteases, which stimulate Gq-coupled PAR receptors. In airway epithelia, PAR2 receptors have been reported to activate store-operated Ca^{2+} channels through InsP_3 -driven Ca^{2+} store depletion (Jairaman et al., 2016).

Our data show that mite extract activates both PAR2 and PAR4 receptors in mast cells but PAR4 activation couples more strongly to store-operated Ca^{2+} entry. Stimulation with mite extract evoked bi-phasic Ca^{2+} release: an initial large, rapid Ca^{2+} transient was followed by a smaller but considerably more prolonged Ca^{2+} mobilization phase. The integrated Ca^{2+} signal for the second phase was ~2-fold greater than the first phase, reflecting its longer duration. Our pharmacological studies showed that the first phase arose from activation of PAR2 receptors whereas the second phase was a consequence of PAR4 stimulation. Both phases of Ca^{2+} release were prevented by inhibition of phospholipase C or by prior depletion of the Ca^{2+} store with thapsigargin. Therefore PAR2 and PAR4 receptors stimulate Ca^{2+} release via InsP_3 -dependent Ca^{2+} mobilization from the ER. Nevertheless, the receptors were not equally efficacious in activating store-operated Ca^{2+} entry. Several pieces of evidence suggest that the PAR4-mediated slow second phase of Ca^{2+} release was particularly relevant for CRAC channel activation. First, an increase in the amplitude of the second phase translated into stronger stimulation of store-operated Ca^{2+} entry, as expected for a Ca^{2+} influx pathway that is contingent on the extent of store depletion. By contrast, there was a poor correlation between the size of the PAR2-mediated first phase of Ca^{2+} release and subsequent Ca^{2+} entry. Second, loss of functional PAR2 receptors by trypsin-mediated desensitization or application of a PAR2-specific antagonist abolished the first phase of Ca^{2+} release but the second phase and store-operated Ca^{2+} entry were unaffected. Third, block of PAR4 receptors had no effect on the first phase of Ca^{2+} release but the second phase and store-operated Ca^{2+} entry were suppressed. Fourth, boiling house dust mite extract had no effect on the first phase of Ca^{2+} release but the second phase as well as CRAC channel activation were inhibited. The difference in coupling between PAR2 and PAR4 receptor activation and store-operated Ca^{2+} entry might reflect the rapid homologous desensitization of PAR2 receptors, leading to a fast but transient burst of InsP_3 production. This would result in transient Ca^{2+} release and rapid store refilling due to the decline in InsP_3 and therefore translate into weak activation of CRAC channels. By contrast, the more sustained Ca^{2+} release response to PAR4 stimulation indicates prolonged Ca^{2+} release and therefore sufficient store emptying for CRAC channel activation. In more general terms, our data show that different members of the same receptor family activate CRAC channels to very different extents in the same cell type. Such 'selective coupling' will enable the same agonist to evoke different cytosolic Ca^{2+} signatures depending on which receptor subtype is activated.

The combination of pharmacologic inhibitors, fractionation and mass spectrometry identified Der p3 as the major serine protease that activated CRAC

channels. Der p3 is produced in the gut of *Dermatophagoides Pteronyssinus* as an inactive pro-enzyme, which is then cleaved by the cysteine protease Der p1 to release active Der p3. Cleavage of recombinant pro-Der p3 by either mite extract or recombinant Der p1 resulted in robust Ca^{2+} influx. *Dermatophagoides Pteronyssinus* contains at least 23 Der p allergens. It is therefore remarkable that just one, Der p3, can activate store-operated Ca^{2+} entry. This should not be taken to imply that the other allergens are unimportant in terms of signalling; house dust mite extract-dependent membrane protrusion and cell migration were both only partially reduced despite full inhibition of Ca^{2+} influx. Because these responses were suppressed completely by boiling the extract, other components within the mite extract contribute to these responses independent of Ca^{2+} influx.

Mutagenesis studies on the catalytic triad of Der p3 as well as the effects of structurally distinct serine protease inhibitors demonstrate that enzyme activity is required for Der p3 activation of the Ca^{2+} channels. The serine protease inhibitor nafamostat, which we have shown suppresses Der p3 activity, reduces *Dermatophagoides Pteronyssinus*-induced airway inflammation in a murine model of asthma (Chen et al., 2006). High doses of nafamostat have also been used clinically as an anti-coagulant in hemodialysis (Davenport, 2011), although widespread use in the clinic is tempered by a report that nafamostat can lead to anaphylactic shock (Maruyama et al., 1996). Targeting store-operated Ca^{2+} channels is clearly of benefit in dampening down the severity of allergic asthma in animal models of the disease (Ohga et al., 2008; Sutovska et al., 2016). However, in light of the numerous roles that store-operated Ca^{2+} influx fulfils in cells, an attractive approach would be to target both Der p3 and CRAC channels, but with sub-maximal inhibition of each. The combination should effectively prevent Der p3-induced activation of Ca^{2+} signalling, whilst both preserving sufficient CRAC channel activity for normal cell function and reducing the likelihood of off-target effects of nafamostat. Indeed, we find that the combination of sub-maximal doses of a CRAC channel blocker and nafamostat is very effective in suppressing house dust mite-driven Ca^{2+} signalling, opening up an additional approach for treating asthma.

Figure legends.

Figure 1. Mite whole body extract evokes Ca^{2+} release and Ca^{2+} influx in various cell types associated with asthma. **A**, Extract applied in Ca^{2+} -free external solution to human nasal mast cells triggered Ca^{2+} release followed by Ca^{2+} influx when external Ca^{2+} was readmitted (trace is mean of 13 cells). The response to thapsigargin (mean of 10 cells) is also shown. Arrows indicate addition of external Ca^{2+} . **B**, Mite extract elicited Ca^{2+} signals in RBL-2H3 cells, and in a dose-dependent manner. **C**, The rate of Ca^{2+} entry to mite extract in RBL-2H3 cells is compared with the corresponding response induced by 2 μM thapsigargin (100%). Bars denote 81 cells for thapsigargin and 83 cells for mite extract. **D**, Mite extract evokes Ca^{2+} signals in human bronchial airway epithelial cells. The background signal, where cells were perfused with Ca^{2+} -free solution and then external Ca^{2+} readmitted but all in the absence of mite extract, is shown in grey. **E**, Dose-dependent Ca^{2+} signals to mite extract are shown from HEK-293 cells. **F**, Table summarises mite-evoked responses in the various cell types tested. BMDC denotes bone marrow-derived mast cells. **G**, Ca^{2+} release to mite extract is suppressed by U73122 (10 μM ; 5 minutes pre-treatment). Extract was applied in

Ca²⁺-free solution. HDM trace denotes 25 cells and HDM + U73122 30 cells. **H**, Expression of the cytosolic InsP₃ binding protein (IP₃-Buffer) significantly reduces Ca²⁺ release to mite extract. Wild-type trace is the mean of 14 cells and IP₃-buffer denotes 17 cells. **I**, Mite extract fails to release Ca²⁺ following prior exposure to thapsigargin (2 μ M). Averaged data from 9 cells are shown. For the graphs, all data are presented as Mean \pm SEM.

Figure 2. Mite extract activates CRAC channels. **A**, Store-operated Ca²⁺ entry evoked by thapsigargin (2 μ M) is compared with mite extract-induced Ca²⁺ influx. Cells were stimulated in Ca²⁺-free solution and then external Ca²⁺ readmitted (arrows). **B**, Pharmacological profile of thapsigargin-induced Ca²⁺ influx. Each bar is the mean of between 21 and 35 cells. **C**, Pharmacological profile of mite extract-induced Ca²⁺ influx. Each bar is the mean of between 21 and 40 cells. Doses used were as follows: La³⁺ 50 μ M, 2-APB 30 μ M, BTP2 10 μ M, Synta 66 10 μ M. Mite extract was 400 μ g/ml. **D**, Ba²⁺ entry increases significantly following challenge with mite extract. The background trace denotes Ba²⁺ entry in the absence of exposure to mite extract. **E**, Ca²⁺ influx to mite extract is shown in cells bathed in 100 mM K⁺-solution. Corresponding background trace in 100 mM K⁺-solution is shown. 5 mM external Ca²⁺ was used to compensate partially for the fall in the electrical gradient for Ca²⁺ entry. **F**, Whole cell patch clamp recording is shown. Mite extract was applied shortly before break-in in Ca²⁺-free solution and 10 mM Ca²⁺ was added as shown. **G**, Current-voltage relation of the current in panel F is shown, taken at steady state after Ca²⁺ had been readmitted. Superimposed is the current-voltage relationship after dialysis with InsP₃ (30 μ M) from another cell. **H**, Bars compare the size of the CRAC current (I_{CRAC}) for the conditions shown. Each bar is the mean of between 4 and 9 cells. All cells used in this Figure were RBL-2H3 cells. For the graphs, all data are presented as Mean \pm SEM.

Figure 3. Mite extract activates PAR2 and PAR4 receptors, with the latter coupling to Ca²⁺ entry. **A**, Ca²⁺ responses to mite extract fall into three groups, depending on the size of the second phase of Ca²⁺ release: big, medium and small. **B**, The graph compares the size of the second phase with the rate of Ca²⁺ entry. **C**, PAR receptor expression in RBL-2H3 cells is compared. **D**, Trypsin (0.1 mg/ml) triggers Ca²⁺ release followed by Ca²⁺ influx. Trypsin trace is mean of 12 cells and background trace 15 cells. **E**, The initial fast phase of Ca²⁺ release induced by mite extract is lost after trypsin receptor desensitization, but the second slow phase and store-operated Ca²⁺ entry are unaffected. Control HDM trace is the mean of 37 cells and trypsin-HDM the mean of 24 cells. **F**, The PAR2 receptor antagonist FSLLRY-NH₂ (500 μ M; 30 minutes pre-incubation) inhibits the initial fast phase of Ca²⁺ release to mite extract, but not the second slow phase or store-operated Ca²⁺ entry. Traces are means of 10 (HDM) and 9 (FSLLRY-NH₂ + HDM) cells. **G**, Thrombin (25 μ M) releases Ca²⁺ from internal stores, followed by Ca²⁺ influx. Trace is mean of 20 cells. Inset shows dose-response curve to thrombin. Ca²⁺ release was measured. **H**, The PAR4 antagonist ML354 (3 μ M; 15-20 minutes pre-incubation) inhibits Ca²⁺ release and Ca²⁺ influx to thrombin. **I**, ML354 has no effect on Ca²⁺ signals to trypsin. Trypsin trace is the mean of 31

cells and ML354+ trypsin 20 cells. **J**, ML354 has no effect on the initial fast phase of Ca^{2+} release induced by mite extract but abolishes the second slow component and store-operated Ca^{2+} entry. HDM trace is the mean of 20 cells, ML354 + HDM denotes mean of 19 cells and background is mean of 7 cells. **K**, The PAR4 peptide agonist AYPGFK-NH₂ (denoted AY-NH₂) triggers dose-dependent Ca^{2+} release followed by Ca^{2+} entry. **L**, Ca^{2+} release and subsequent Ca^{2+} entry to AY-NH₂ (30 μM) is prevented by U73122. BTP2 (10 μM) abolishes Ca^{2+} entry. Each trace is the mean of 11-13 cells. **M**, FACS analysis shows that pre-treatment with house dust mite reduces fluorescein-coupled PAR4 peptide agonist binding. Upper panel denotes RBL-2H3 cells not exposed to fluorescein-coupled PAR4 agonist. – denotes fluorescein-negative cells (99.8%) and + denotes fluorescein-positive cells (0.22%). Middle panel shows the profile after application of fluorescein-conjugated peptide. 91.7% of cells were now fluorescein-positive and 8.3% were fluorescein-negative. The lower panel depicts the profile to fluorescein-conjugated peptide after exposure to house dust mite extract. Fluorescein-positive cells were reduced to 67.5% and fluorescein-negative cells increased to 32.5%. For the graphs, all data are presented as Mean \pm SEM.

Figure 4. Ca^{2+} influx to mite extract requires STIM1 gating of Orai1. **A**, Western blots compare STIM1 and Orai1 protein expression before and after knockdown. **B**, Aggregate data from two independent experiments are shown. **C**, Mite-induced Ca^{2+} influx is reduced following knockdown of either STIM1 or Orai1. **D**, Aggregate data from several experiments as in panel C are compared. HDM (400 $\mu\text{g}/\text{ml}$) is the mean of 159 cells, KD STIM1 126 cells and KD Orai1 81 cells. **E**, TIRF images of STIM1-YFP puncta are compared between resting HEK-293 cells and cells stimulated with mite extract. Images for the stimulated condition were taken 9 minutes after mite exposure in Ca^{2+} -free solution. **F**, Confocal images compare STIM1-YFP distribution in HEK-293 cells at rest, after stimulation with thapsigargin (8 minutes) and after exposure to mite extract (15 minutes). **G**, The rate of Ca^{2+} entry, normalised to control (mock-transfected cells), is compared for the conditions shown. HDM bar denotes mean of 44 cells, STIM1 38 cells and STIM1+Orai1 30 cells. **H**, Aggregate data are compared. Orai1 was knocked down and then the various constructs indicated were expressed (together with STIM1) 24 hours later. GFP bar denotes mean of 66 cells (which were transfected only with GFP plasmid and served as control), - 52 cells, Orai1 33 cells, L273S-Orai1 37 cells and ⁸¹AARAE⁸⁵-Orai1 15 cells. For the graphs, all data are presented as Mean \pm SEM.

Figure 5. Der p3 regulates CRAC channels. **A**, Boiling mite extract suppresses the second slow phase of Ca^{2+} release and store-operated Ca^{2+} influx. **B**, Aggregate data are compared. HDM (400 $\mu\text{g}/\text{ml}$) trace is mean of 21 cells and boiled HDM 41 cells. **C**, Serine protease inhibitors reduce mite extract-evoked Ca^{2+} entry. Mite extract was pre-mixed with each inhibitor for 20 minutes before application to cells. HDM group denotes mean of 43 cells, nafamostat (10 μM) 57 cells, camostat (500 μM) 24 cells, aprotinin (10 μM) 95 cells and E-64 (10 μM) 69 cells. **D**, The effect of mite extract fractions on Ca^{2+} entry is compared. The background trace denotes Ca^{2+} influx in cells exposed to Ca^{2+} -free solution for the same time. The background is the same in all three traces because each fractionation experiment was run on the same day. **E**, Coomassie blue gel of the fractions

shown in panel D. **F**, Heat map summarises which Der p proteins were present in each fraction, detected by mass spectrometry analysis. **G**, Western blot shows cleavage of pro-Der p3 by a low dose of mite extract and that this is prevented by pre-treatment with E-64. **H**, Bacteria-purified pro-Der p3 (6 μ g) and a low dose of house dust mite extract (30-60 μ g/ml) each fail to elicit Ca^{2+} influx, but their combination (pre-mixed at 37°C for 10-20 minutes) evokes prominent Ca^{2+} entry. Pro-Der p3 trace is mean of 12 cells, low HDM 20 cells and pro-Der p3 + low HDM 11 cells. **I**, Ca^{2+} entry is inhibited when pro-Der p3 is mutated at the pro-cleavage site such that cleavage of the pro-form is impaired. Each bar is the mean of > 15 cells. The cleavage sequence of original (uncut) Der p3 and uncut Der p3 are shown at the top of the panel. Mutated amino acids are shown in red. The signal sequence has been removed after methionine for simplicity. **J**, Ca^{2+} influx to the combination of pro-Der p3 and a low dose of mite extract is suppressed by either pre-treatment of mite extract with E-64 (labelled E-64+ Low HDM; pro-Der p3) or knock down of Orai1. Addition of E-64 after pro-der p3 had been incubated with mite extract for ~10 minutes had no inhibitory effect (labelled Low HDM + pro-Der p3; E-64). Each trace is the mean of between 8 and 23 cells. All data are from RBL-2H3 cells except panel H, which was from HEK-293 cells. For the graphs, all data are presented as Mean \pm SEM.

Figure 6. Catalytic activity of Der p3 is required for Ca^{2+} entry. **A**, Pre-treatment with nafamostat prevents Ca^{2+} influx to the combination of a low dose of mite extract (30 μ g/ml) and pro-Der p3 (6 μ g; trace labelled nafamostat; L.D. HDM+pro-Der p3). Nafamostat suppressed Ca^{2+} influx when applied after mite extract had been mixed with pro-Der p3 for ~10 minutes (L.D. HDM+pro-Der p3; nafamostat). **B**, Addition of Der p3 proteins with mutations within the catalytic triad to a high dose of mite extract abolishes Ca^{2+} influx. **C**, Incubation of commercially available Der p1 (10 μ g) with pro-Der p3 enhance Ca^{2+} influx, compared with either Der p1 or pro-Der p3 alone. Ca^{2+} entry to the combination of Der p1 and pro-Der p3 is inhibited by either E-64 or nafamostat. **D**, The combination of a low dose of mite extract and commercial pro-Der p3 enhances Ca^{2+} influx. **E**, The combination of sub-maximal doses of nafamostat (1 μ M) and BTP2 (5.5 μ M) suppresses Ca^{2+} influx to a low dose of mite extract pre-incubated with pro-Der p3, whereas each inhibitor alone has only a partial effect. **F**, Aggregate data are summarised. Each bar denotes between 14 and 22 cells. For the graphs, all data are presented as Mean \pm SEM.

Figure 7. Mite extract induces mast cell membrane protrusions and cell migration. **A**, Trans-illumination images show protrusions (marked by arrows) on the surface of RBL-2H3 cells within minutes of mite extract exposure. Rest denotes non-stimulated condition. **B**, The % of cells that develop protrusions to mite extract are compared for the conditions shown. Rest denotes the mean of 33 cells, HDM alone 75, cyto D 29, 0 Ca^{2+} 96, BTP2 25, U73122 55 **C**, Electron micrographs compare a resting cell and one challenged with mite extract for 15 minutes before fixation. **D**, Transwell assay compares RBL-2H3 cell migration at rest and after mite extract exposure (16-18 hours). **E**, Aggregate data from three independent conditions are compared. Data are normalised to migration induced by mite extract (second bar). **F**, Cytosolic Ca^{2+} signals from bone marrow-derived mast cells are shown following stimulation with thapsigargin or mite extract.

Each trace is the mean of 14-23 cells. **G**, Aggregate data from bone marrow-derived mast cells are compared for the conditions shown. **H**, Transwell assay compares bone marrow-derived mast cell migration between resting (non-stimulated) cells and cells exposed to mite extract for 18 hours. **I**, Aggregate data from 2 separate experiments are shown. For the graphs, all data are presented as Mean \pm SEM.

Acknowledgments. This work was supported by an American Asthma Senior Investigator Award to A.B.P. and MRC Programme Grant (LO1047X) to A.B.P.. We acknowledge the Computational Biology Research Group (CBRG) for maintenance of the MASCOT proteomics server. CBRG is supported by a MRC Strategic Award to the institute.

Author Contributions

A.B.P. designed the project. Y-P.L performed experiments and affiliated analyses. C.N. performed electron microscopy. Y-P.L and H.K. performed mass spectrometry experiments and analysis. A.B.P. conducted patch clamp experiments, supervised the project and wrote the paper.

Declaration of Interest

ABP is Scientific Founder of CalciCo Therapeutics and sits on the Board of Directors.

References

- Anandan, C., Nurmatov, U., van Schayck, O.C., and Sheikh, A. (2010). Is the prevalence of asthma declining? Systematic review of epidemiological studies. *Allergy* 65, 152–167.
- Azofra, J., and Lombardero, M. (2003). Limpet anaphylaxis: cross-reactivity between limpet and house-dust mite *Dermatophagoides pteronyssinus*. *Allergy* 58, 146-149.
- Baba, Y., Nishida, K., Fujii, Y., Hikida, M., and Kurosaki, T. (2008). Essential function for the calcium sensor STIM1 in mast cell activation and anaphylactic responses. *Nature Immunology* 9, 81-88.
- Bakowski, D., and Parekh, A.B. (2007). Voltage-dependent Ba²⁺ permeation through store-operated CRAC channels: implications for channel selectivity. *Cell Calcium* 42, 333-339.
- Bousquet, P.J., Chinn, S., Janson, C., Kogevinas, M., Burney, P., Jarvis, D., and I., E.C.R.H.S. (2007). Geographical variation in the prevalence of positive skin tests to environmental aeroallergens in the European Community Respiratory Health Survey I. *Allergy* 62, 301-309.
- Chen, C.-L., Wang, S.-D., Zeng, Z.-Y., Lin, K.-J., Kao, S.-T., Tani, T., Yu, C.-K., and Wang, J.-Y. (2006). Serine protease inhibitors nafamostat mesilate and gabexate mesilate attenuate allergen-induced airway inflammation and eosinophilia in a murine model of asthma. *Journal of Allergy and Clinical Immunology* 118.
- Chew, G.L., Reardon, A.M., Correa, J.C., Young, M., Acosta, L., Mellins, R., Chew, F.T., and Perzanowski, M.S. (2009). Mite sensitization among Latina women in New York, where dust-mite allergen levels are typically low.
- Chew GL, Reardon AM, Correa JC, Young M, Acosta L, Mellins R, Chew FT, Perzanowski MS. *Indoor Air*. 2009 Jun;19(3):193. *Indoor Air* 19, 193-197.

Coughlin, S.R. (2000). Thrombin signalling and protease-activated receptors. *Nature* 407, 258-264.

Davenport, A. (2011). What are the anticoagulation options for intermittent hemodialysis? *Nature Rev Nephrol* 7, 499-508.

Di Capite, J., Nelson, C., Bates, G., and Parekh, A.B. (2009). Targeting CRAC channels and leukotriene receptors provides a novel combination strategy for treating nasal polyposis. *Journal of Allergy and Clinical Immunology* 124, 1014-1021.

Dumez, M.-E., Teller, N., Mercier, F., Tanaka, T., Vandenberghe, I., Vandendyck, M., Devreese, B., Luxen, A., Fre`re, J.-M., Matagne, A., *et al.* (2008). Activation Mechanism of Recombinant Der p 3 Allergen Zymogen. *Journal of Biological Chemistry* 283, 30606-30617.

Faruqi, T.R., Weiss, E.J., Shapiro, M.J., Huang, W., and Coughlin, S.R. (2000). Structure-function analysis of protease-activated receptor 4 tethered ligand peptides. Determinants of specificity and utility in assays of receptor function. *Journal of Biological Chemistry* 275, 19728-19734.

French, S.I., and Hamilton, J.R. (2016). Protease-activated receptor 4: from structure to function and back again. *British Journal of Pharmacology* 173, 2952-2965.

Gøtzsche, P.C., Johansen, H.K., Schmidt, L.M., and Burr, M.L. (2004). House dust mite control measures for asthma. *Cochrane Database Syst Rev* 4, CD001187.

Gregory, L.G., and Lloyd, C.M. (2011). Orchestrating house dust mite-associated allergy in the lung. *Trends in Immunology* 32, 402-411.

Gudlur, A., Quintana, A., Zhou, Y., Hirve, N., Mahapatra, S., and Hogan, P.G. (2014). STIM1 triggers a gating rearrangement at the extracellular mouth of the ORAI1 channel. *Nature Communications* 5, 5164.

Hammad, H., and Lambrecht, B.N. (2015). Barrier Epithelial Cells and the Control of Type 2 Immunity. *Immunity* 43, 29-40.

Holgate, S.T. (2013). Immune circuits in asthma. *Curr Opin Pharmacol* 13, 345-350.

Illi, S., von Mutius, E., Lau, S., Niggemann, B., Grüber, C., Wahn, U., and group., M.A.S.M. (2006). Perennial allergen sensitisation early in life and chronic asthma in children: a birth cohort study. *Lancet* 368, 763-770.

Jairaman, A., Maguire, C.H., Schleimer, R.P., and Prakriya, M. (2016). Allergens stimulate store-operated calcium entry and cytokine production in airway epithelial cells. *Scientific Reports* 6, 32311.

Lewis, R.S., and Prakriya, M. (2015). Store-Operated Calcium Channels. *Physiological Reviews* 95, 1383-1436.

Maruyama, H., Miyakawa, Y., Gejyo, F., and Arakawa, M. (1996). Anaphylactoid reaction induced by nafamostat mesilate in a hemodialysis patient. *Nephron* 74, 468-469.

Ohga, K., Takezawa, R., Yoshino, T., Yamada, T., Shimizu, Y., and Ishikawa, J. (2008). The suppressive effects of YM-58483/BTP2, a store-operated Ca²⁺ entry blocker, on inflammatory mediator release in vitro and airway responses in vivo. *Pulmonary Pharmacology and Therapeutics* 21, 360-369.

Parekh, A.B. (2010). Store-operated CRAC channels: function in health and disease. *Nature Reviews Drug Discovery* 9, 399-410.

Pawankar, R. (2014). Allergic diseases and asthma: a global public health concern and a call to action. *World Allergy Organ J* 7, 12.

Platts-Mills, T.A., Vervloet, D., Thomas, W.R., Aalberse, R.C., and Chapman, M.D. (1997). Indoor allergens and asthma: report of the Third International Workshop. *Journal of Allergy and Clinical Immunology* 100, S2-S4.

Singaravelu, K., Nelson, C., Bakowski, D., de Brito, O.M., Ng, S.W., Di Capite, J., Powell, T., Scorrano, L., and Parekh, A.B. (2011). Mitofusin 2 regulates STIM1 migration from the Ca²⁺ store to the plasma membrane in cells with depolarised mitochondria. *Journal of Biological Chemistry* 286, 12189-12201.

Spergel, J.M., and Paller, A.S. (2003). Atopic dermatitis and the atopic march. *Journal of Allergy and Clinical Immunology* 112, S118-127.

Sutovska, M., Kocmalova, M., Franova, S., Vakkalanka, S., and Viswanadha, S. (2016). Pharmacodynamic evaluation of RP3128, a novel and potent CRAC channel inhibitor in guinea pig models of allergic asthma. *European Journal of Pharmacology* 772, 62-70.

Vig, M., DeHaven, W.I., Bird, G.S., Billingsley, J.M., Wang, H.J., Rao, P.E., Hutchings, A.B., Jouvin, M.H., Putney, J.W., and Kinet, J.P. (2008). Defective mast cell effector functions in mice lacking the CRACM1 pore subunit of store-operated calcium release-activated calcium channels. *Nature Immunology* 9, 89-96.

Von Mutius, E. (2009). Gene-environment interactions in asthma. *Journal of Allergy and Clinical Immunology* 123, 3-11.

STAR Methods

KEY RESOURCES TABLE

REAGENT or RESOURCE	SOURCE	IDENTIFIER
Antibodies		
Anti-STIM1	Cell Signaling	5668
Anti-Orai1	Santa Cruz	sc-68895
Anti-His	Santa Cruz	sc-8036
Bacterial and Virus Strains		
BL21(DE3), E.coli	Lucigen	60401-2
Biological Samples		
Human nasal mast cells	ENT Department	
Chemicals, Peptides, and Recombinant Proteins		
Der p1 protein	Indoor Biotechnologies	RP-DP1D-1
Der p3 protein	Bioclone Inc.	PQ-0335
House dust mite	Greer	XPB70D3A2.5
Nafamostat mesylate	Sigma	N0289
Camostat mesylate	Sigma	SML0057
Aprotinin	Sigma	A1153
E-64	Sigma	E3132
U73122	TOCRIS	1268
Thapsigargin	Merck	67526-95-8
BTP2		
2-APB	Sigma	D9754
Synta-66		
Fura-2-AM	Life technologies	F-1221
AYPGKF- NH2	Sigma	A3327
ML354	Sigma	SML1439
Benzoyl-L-arginine p-nitroanilide hydrochloride	Sigma	B3133
Recombinant murine IL-3	PEPROTECH	AF-213-13
Critical Commercial Assays		
Deposited Data		
http://dx.doi.org/10.17632/46z5yp68dz.1		
Experimental Models: Cell Lines		
RBL-2H3	ATCC	
HEK-293	ATCC	
16HBE	Dr. Ling-Pei Ho	Oxford University
Jurkat T cells	Dr. Daniel Bakowski	Calcico Therapeutics
BMMC isolated from C57BL/6 mice	Department of Biomedical Services	Oxford University
Experimental Models: Organisms/Strains		
-		

Oligonucleotides		
siRNA for STIM1	Life Technologies	4390815
siRNA for Orai1	OriGene	SR508429
Primers for rat PAR1-4: PAR-1: Sense: 5'-GCTACTACTTCTCCGGCACC-3' Antisense: 5'- ATGACCACGCAGGTGAAGTT-3' PAR-2: Sense: 5'-CACCACCTGTCACGACGTGCT-3' Antisense: 5'-CTCAGTAGGAGGTTTTAACAC-3' PAR-3: Sense: 5'- GCCCCACCAACATCATACT-3' Antisense: 5'- AATAAAGGAATGGGTCTAGGCAA-3 PAR-4: Sense: 5'-TAGAACTTAATGAGTCGAAG-3' Antisense: 5'-CACTGAACCATACATGTGGC-3'	This paper	
Primers for human PAR1-4: PAR-1: Sense: 5'-TGTGAACTGATCATGTTTATG-3' Antisense: 5'-TTCGTAAGATAAGAGATATGT-3' PAR-2: Sense: 5'-AGAAGCCTTATTGGTAAGGTT-3' Antisense: 5'-AACATCATGACAGGTCGTGAT-3' PAR-3: Sense: 5'-CTGATACCTGCCATCTACCTCC-3' Antisense: 5'-AGAAAAGTGTGGCCACACC-3' PAR-4: Sense: 5'-ATTACTCGGACCCGAGCC-3' Antisense: 5'-TGTAAGGCCACCCCTTCTC-3'	This paper	
Recombinant DNA		
STIM1-YFP	Dr. T. Meyer	Stanford University
Orai1-CFP	Dr. J. Putney	NIEHS, USA
IP ₃ -buffer	Dr. Maria de Fatima Leite	Federal University of Minas Gerais, Brazil
L273S-Orai1	Made in lab	
AARAE-Orai1	Dr P. Hogan	UCSD, USA
His-tagged pro-Der p3	Bioclone Inc.	RPQ-0335
S214A-pro-Der p3 mutant	Mutagenex	
D114A-pro-Der p3 mutant	Mutagenex	
Sequence for generation uncut-Der p3	This paper	
Software and Algorithms		
-		
Other		
-		

Contact for Reagent and Resource Sharing

Contact should be directed to the corresponding author, Anant Parekh
(anant.parekh@dpag.ox.ac.uk)

Experimental Model and Subject Details

Cell Culture and Maintenance

Human nasal mast cells were obtained after surgical removal from patients with nasal polyposis and used shortly after excision (Di Capite et al., 2009). Full

patient consent was provided and approval was from the National Research Ethics Service (REC no./07/H0607/104). RBL-2H3 and HEK-293 cells were purchased from ATCC. The human bronchial airway epithelial cell line 16-HBE and Jurkat T cells were kind gifts from Dr Ling-Pei Ho (Weatherall Institute of Molecular Medicine, Oxford) and Dr Daniel Bakowski (Calcico Therapeutics, Oxford). RBL-2H3 and HEK-293 cells were cultured at 37°C with 5% CO₂ in DMEM supplemented with 10% fetal bovine serum and penicillin/streptomycin. 16-HBE cells were cultured (37°C, 5% CO₂) in Dulbecco's modified Eagle's medium with 10% fetal bovine serum, 2 mm l-glutamine, and penicillin/streptomycin. Jurkat T cells were cultured (37°C, 5% CO₂) in RPMI with 10% fetal bovine serum.

Bone marrow-derived mast cells were isolated from the femurs of C57BL/6 adult mice. The cells were cultured at 37°C in an incubator containing 5% CO₂ in DMEM medium supplemented with 10ng/ml interleukin-3, 10% FBS and 1% penicillin/streptomycin. After 4 weeks differentiation, the percentage of mast cells was >95% mast cells, as measured by flow cytometry of FcεRI receptor expression.

Plasmids and Transfection

RBL-2H3 cells were transfected using the Amaxa electroporation system. All other cell types were transfected using lipofectamine. cDNA for STIM1-YFP was a gift from Dr T. Meyer (Stanford University), Orai1-CFP was from Dr J. Putney (NIEHS, NIH) and InsP₃ buffer was from Dr. Maria de Fatima Leite (Federal University of Minas Gerais, Brazil).

siRNA to STIM1 was purchased from ambion and had the following sequences

(5'-3'): Sense CCAUGACCCUACAGUGAAAtt

(5'-3'): Antiense UUUCACUGUAGGGUCAUGGta

siRNA to Orai1 comprised 3 unique 27mer duplexes from OriGene and had the following sequences:

SR508429A-rArGrUrUrCrUrUrArCrCrGrCrUrCrArArGrArGrGrCrArGGC

SR508429B-rCrCrArUrArArGrArCrGrGrArCrCrGrArCrArGrUrUrCrCAG

SR508429C-rArGrGrGrCrArGrArGrUrGrUrGrGrArArGrGRArArGrArGGC

Site-directed mutagenesis

The S214A-pro-Derp3 and D114A-pro-Derp3 mutant plasmids were provided by Mutagenex from his-tagged pro-Derp3 plasmid which was purchased from Bioclone Inc. The activation of the his-tagged pro-Derp3 requires the cleavage of the pro-peptide to form active Der p3 (Dumez et al., 2008). A mutant Der p3 in which the pro-peptide could not be cut was made using QuikChangeSite-Directed Mutagenesis Kit (Agilent). The primers used for generating the mutations in the pro-peptide cleavage site were 5'-tggtggtggtgctcgagcgcttgagaacgttagattcaatc-3' and 5'-gattgaatctaaacgttctcaagcgctcgagcaccaccacca-3' and then 5'-agaagcaggcaggattggagccatattggccttggaagtac-3' and 5'-gtacttccaaggccatattgctccaatcctgctgttct-3'.

House dust mite extract and recombinant proteins

Dermatophagoides Pteronyssinus whole body extract was bought from Greer laboratories. Der p1 was from Indoor Biotechnologies (USA) and both pro-Der p3 plasmid and protein were from Bioclone Inc..

Cytosolic Ca²⁺ measurements

Cytosolic Ca²⁺ measurements were carried out at room temperature using the IMAGO charge-coupled device camera-based system from TILL Photonics (Kar et al., 2012). Cells were loaded with Fura-2/AM (1 μ M) for 40 minutes in the dark and then allowed to stand for 15 minutes for complete dye de-esterification. Cells were alternately excited at 356 and 380 nm (20 ms exposures) at 0.5 Hz. Standard external solution contained 145 mM NaCl, 2.8 mM KCl, 2 mM CaCl₂, 2 mM MgCl₂, 10 mM D-glucose and 10 mM HEPES (pH 7.4 with NaOH). Ca²⁺-free solution had the same composition but CaCl₂ was omitted and 0.1 mM Ethylene glycol-bis(b-aminoethyl ether)-N,N,N',N'-tetraacetic acid (EGTA) added. Cytosolic Ca²⁺ signals are plotted as R, which denotes the 356/380 nm ratio. We quantified Ca²⁺ influx by measuring the rate of rise of cytosolic Ca²⁺ following readmission of external Ca²⁺, as this more accurately reflects Ca²⁺ channel activity than the steady-state cytosolic Ca²⁺ signal since the latter is sculpted not only by Ca²⁺ influx but also by the rate of Ca²⁺ removal from the cytosol (Parekh and Penner, 1997).

TiRF microscopy

HEK-293 cells expressing STIM1-YFP were illuminated with 488-nm laser light. Light reflected from the back focal plane was detected with a x100 oil-immersion objective, and images were captured with 1 x 1 pixel binning. YFP fluorescence was measured before and then after stimulation with mite extract or thapsigargin for each cell. YFP fluorescence was measured in Image J.

PAR4 receptor activation

The PAR4 peptide agonist AYPGKF-NH₂ conjugated with fluorescein was purchased from Sigma-Aldrich. For FACS analysis (Figure 3), RBL-2H3 cells were detached using 10mM EDTA for 10 min at 37°C. After washing twice with PBS, cells were treated with or without dust mite extract for 10 minutes, then incubated with 100 μ M fluorescein-conjugated PAR4 agonist peptide for 15 minutes. Cells were then washed several times with PBS and then the fluorescence intensity at 488 nm was detected by FACScan™ flow cytometer (BD Biosciences) and analyzed by FlowJo software. For immuno-fluorescence, RBL-2H3 cells were washed with PBS twice, then incubated with 100 μ M fluorescein peptide for 15 minutes. The cells were then washed, fixed with 4% paraformaldehyde, then washed again several times with PBS. The cell surface fluorescence intensity of the peptide was detected using an Olympus BX51W1 microscope. Control cells were not exposed to fluorescein-peptide (background fluorescence), a second group of cells was exposed to fluorescein-peptide and a third group was pre-treated with mite extract for 15 minutes, washed and then exposed to fluorescein-peptide. Fluorescence intensity was measured using Image J. In the experiments using catalytic inactive Der p3, mutant protein was added to mite extract and cells were exposed to this combination for 15 minutes, as for the third group.

Patch clamp recordings

Whole cell patch clamp recordings were carried out in RBL-2H3 cells as previously described (Bakowski and Parekh, 2007). Pipettes were pulled from borosilicate glass, Sylgard-coated and fire-polished. Pipette resistances were in the range 3-4 M Ω when filled with a pipette solution containing 145 mM Cs

glutamate, 8 mM NaCl, 4.6 mM CaCl₂, 10 mM EGTA, 1 mM MgCl₂, 2 mM Mg-ATP and 10 mM HEPES (pH 7.2 with CsOH). Series resistance was < 10 MΩ. Bath solution contained 135 mM NaCl, 2.8 mM KCl, 10 mM CsCl, 2 mM MgCl₂, 0.1 mM EGTA, 10 mM D-glucose and 10 mM HEPES (pH 7.4 with NaOH). In some experiments (see text), InsP₃ (30 μM final concentration) was added to the pipette solution. After 60 seconds dialysis, house dust mite extract was added to the external solution and then after ~ 4 minutes, 10 mM Ca²⁺ was applied.

Western blot

Total cell lysates (50 μg) were separated by SDS-PAGE on a 10% gel and electrophoretically transferred to nitrocellulose membrane, as reported previously (Kar et al., 2014). Membranes were blocked with 5% non-fat dry milk in PBS plus 0.1% Tween 20 (PBST) buffer for 1 hour at room temperature. Membranes were then washed 3 times in PBST and then incubated with primary antibody at 4°C overnight. Anti-STIM1 was from Cell Signalling Technology and used at 1:1000 dilution, anti-his and anti-tubulin were from Santa Cruz and used at 1:2000 and 1:5000, respectively. Membranes were then washed in PBST and then incubated for 1 hour at 4°C with anti-rabbit secondary antibody IgG (1:2500 dilution) or anti-mouse IgG (1:5000 dilution), both from Santa Cruz. After washing again with TBST, the bands were developed for visualization using ECL-plus Western blotting detection system (GE Healthcare). Gels were quantified using Image J.

RT-PCR for protease activated receptor expression

RNA was extracted using an RNeasy Mini Kit (Qiagen). RNA was quantified spectrophotometrically by absorbance at 260 nm. Total RNA (1 μg) was reverse-transcribed using the iScriptTM cDNA Synthesis Kit (Bio-Rad), according to the manufacturer's instructions. After cDNA synthesis, PCR amplification was performed with Go Tag green master mix (Promega) with primers specific for the detection of human protease activated receptors (PAR):

PAR1- Forward: 5'-TGTGAAGTATCATGTTTATG-3'

Reverse: 5'-TTCGTAAGATAAGAGATATGT-3'

PAR2- Forward: 5'-AGAAGCCTTATTGGTAAGGTT-3'

Reverse: 5'-AACATCATGACAGGTCGTGAT-3'

PAR3- Forward: 5'-CTGATACCTGCCATCTACCTCC-3'

Reverse: 5'-AGAAACTGTTGCCCACACC-3'

PAR4- forward: 5'-ATTACTCGGACCCGAGCC-3'

Reverse: 5'-TGTAAGGCCACCCCTTCTC-3'

Primers for RBL-2H3 (rat) cells were:

PAR1- Forward: 5'-GCTACTACTTCTCCGGCACC-3'

Reverse: 5'-ATGACCACGCAGGTGAAGTT-3'

PAR2- Forward: 5'-CACCACCTGTCACGAcGTGCT-3'

Reverse: 5'-CTCAGTAGGAGGTTTAAACAC-3'

PAR3- Forward: 5'-GCCCCACCAACATCATACT-3'

Reverse: 5'-AATAAAGGAATGGGTCTAGGCAA-3'

PAR4- Forward: 5'-TAGAACTtAAtGAGtCGAAG-3'
Reverse: 5'CACTGAACCATACATGTGGC-3'

Liquid chromatography-tandem mass spectrometry.

In-gel trypsin digestion-Protein samples were mixed with reducing SDS-PAGE sample buffer, heat denatured (95°C for 10 min) and resolved on a Tris-Glycine 12% gel. Following Coomassie blue staining each lane was excised to generate 5 equally sized sections which were cut into 1 – 2 mm³ gel pieces and placed into 1.5 mL sample tubes. Gel pieces were rinsed twice with wash solution for 18h in total (200 µL, 50% methanol, 5% acetic acid). The solutions were removed and gel pieces were dehydrated in acetonitrile (200 µL, 5 min). Supernatants were removed and disulfide reduction was performed with 10 mM DTT (30 µL) for 0.5 h, followed by alkylation with 50 mM iodoacetamide (30 µL) for 0.5 h. Supernatants were removed from the gel samples and dehydration with acetonitrile gel pieces were washed with 100 mM ammonium bicarbonate (200 µL, 10 min). Supernatants were removed and dehydration performed with acetonitrile. The gel samples were then rehydrated on ice with freshly prepared trypsin solution (30 µL, 10 ng/µL sequencing grade trypsin [Promega] in 50 mM ammonium bicarbonate). After rehydration excess trypsin solution was removed and 50 mM ammonium bicarbonate (10 µL) was added. Gel samples were digested at 37°C for 18h. The gel pieces were then extracted sequentially with 50mM ammonium bicarbonate (60 µL), 50% acetonitrile, 5% formic acid (60 µL) and 85% acetonitrile, 5% formic acid (60 µL). The combined extracts were evaporated in a vacuum centrifuge and were redissolved in 5% acetonitrile, 0.1% formic acid (20 µL) on an ultrasonic bath, centrifuged (10 min, 5°C, 13,000 g) and transferred into LC-MS sample vials. For the analysis of in-gel digested protein material, liquid chromatography-tandem mass spectrometry (LC-MS/MS) was performed as described previously(Kar et al., 2014). Raw LC-MS/MS data were processed and Mascot compatible files were created using DataAnalysis 4.0 software (Bruker Daltonics). Database searches were performed using the Mascot algorithm(Perkins et al., 1999) (version 2.4) and either the UniProt_SwissProt database with 'other metazoa' taxonomy restriction (v2015.02.04, number of entries: 547 357; after taxonomy filter: 10,242) or the NCBIInr database with 'other metazoa' taxonomy restriction (v2015.02.04, number of entries 59,435,263; after taxonomy filter: 1,185,906). The following parameters were applied: 2+, 3+ and 4+ ions, peptide mass tolerance 0.3 Da, ¹³C = 2, fragment mass tolerance 0.6 Da, number of missed cleavages: two, instrument type: ESI-TRAP, fixed modifications: Carbamidomethylation (Cys), variable modifications: Oxidation (Met).

Electron microscopy

Non-treated (control) and house dust mite treated RBL-2H3 cells were fixed in 4% paraformaldehyde and 0.5% glutaraldehyde in 0.1 M phosphate buffer at pH 7.4 for 2 hr, as described previously(Singaravelu et al., 2011). The same phosphate buffer was also used to wash and postfix the cells in 1% osmium tetroxide for 45 min. Cells were then washed in distilled water and stained with 2% aqueous uranyl acetate for 1 hr. Coverslips were dehydrated through a series of alcohols (30%, 50%, 70%, 90%, and 100%), inverted, and then embedded in

Araldite resin. Once samples had polymerized, coverslips were peeled from the resin, leaving the cells embedded within the resin surface. Whole cells were serially sectioned at 70 nm, via a Reichert ultramicrotome, and collected on formvar-coated grid slots. Grids were post stained with 2% lead acetate and viewed in a Jeol 400 transmission electron microscope.

HDM fractionation (gel filtration chromatography)

Fractionation of house dust mite was done at 4°C using a General Electric AKTA PURIFIER FPLC system. Briefly, 500µl house dust mite was passed through a 0.22µm filter and loaded onto Superose 6 column (GL10/300; GE Healthcare). The column was equilibrated with buffer containing 145 mM NaCl, 2.8 mM KCl, 2 mM CaCl₂, 2 mM MgCl₂, 10 mM D-glucose, and 10 mM Hepes at pH 7.4. The flow rate was 0.3ml/min and one-ml fractions were collected.

Purification of pro-Der p3 protein

Pro-Der p3 plasmid was purchased from Bioclone Inc. Pro-derp3 protein tagged with His6-tagged was produced from Escherichia coli BL21(DE3) and purified on a Histrap HP column (GE Healthcare). Briefly, bacteria were grown in lysogeny broth medium with 1 mM Isopropyl β-D-1-thiogalactopyranoside at 16°C overnight, then lysed by binding buffer (20 mM potassium chloride, 25 mM imidazole, 500mM sodium chloride). After loading into the column, pro-Derp 3 protein was eluted following the percentage increase of elution buffer (20 mM potassium chloride, 500 mM imidazole, 500mM sodium chloride). The protein was further concentrated by use of a VIVASPIN column (Sartorius biotech).

Transwell-cell migration

A transwell migration assay (8 µm pore size, polycarbonate membrane, Corning) was used to test the migratory responses of RBL-2H3 and bone marrow-derived mast cells to house dust mite. RBL-2H3 cells were trypsinised and seeded into the upper chamber with or without house dust mite. After incubation for 16-18 hours at 37°C, cells on the top surface of the membrane were removed and cells that had migrated to the bottom surface of the membrane were fixed and stained by Giemsa staining. Migrated cells in twenty randomly chosen fields of view were counted using ImageJ. Unlike RBL-2H3 cells, the bone marrow-derived mast cells did not attach and therefore migrated cells were in a suspension in the lower chamber. Although bone marrow-derived mast cells migrated when mixed with mite extract in the upper chamber, migration was more robust when mite extract was added to the lower chamber. After spinning down the suspension, we used a cell counter to count the cells. Because this latter method monitored all the cells that had migrated, the absolute cell numbers were larger than for the adherent RBL-2H3 cells. In Figure 7E, which depicts RBL-2H3 cell migration, we normalised migration to the control groups stimulated by mite extract. The absolute number of control cells in this group was $\sim 1.1 \times 10^2$.

Serine protease assay

Serine protease activity of the various Der p3 constructs used in this paper was measured using colorimetric analysis. The substrate *N*_α-Benzoyl-L-arginine *p*-nitroanilide hydrochloride (final concentration of 1.2 mM) was added to Ca²⁺-free external solution (as used in the cytosolic Ca²⁺ measurements above)

supplemented with 100 μ M EGTA in 96 well plates. Der p1 and Der p3 mutants were added to each well, mixed thoroughly and then incubated at 37°C for 15 minutes. The reaction was terminated by addition of 30% acetic acid. The chromophore product p-nitroaniline was detected by colorimetric analysis at 405 nm.

Statistical Analysis

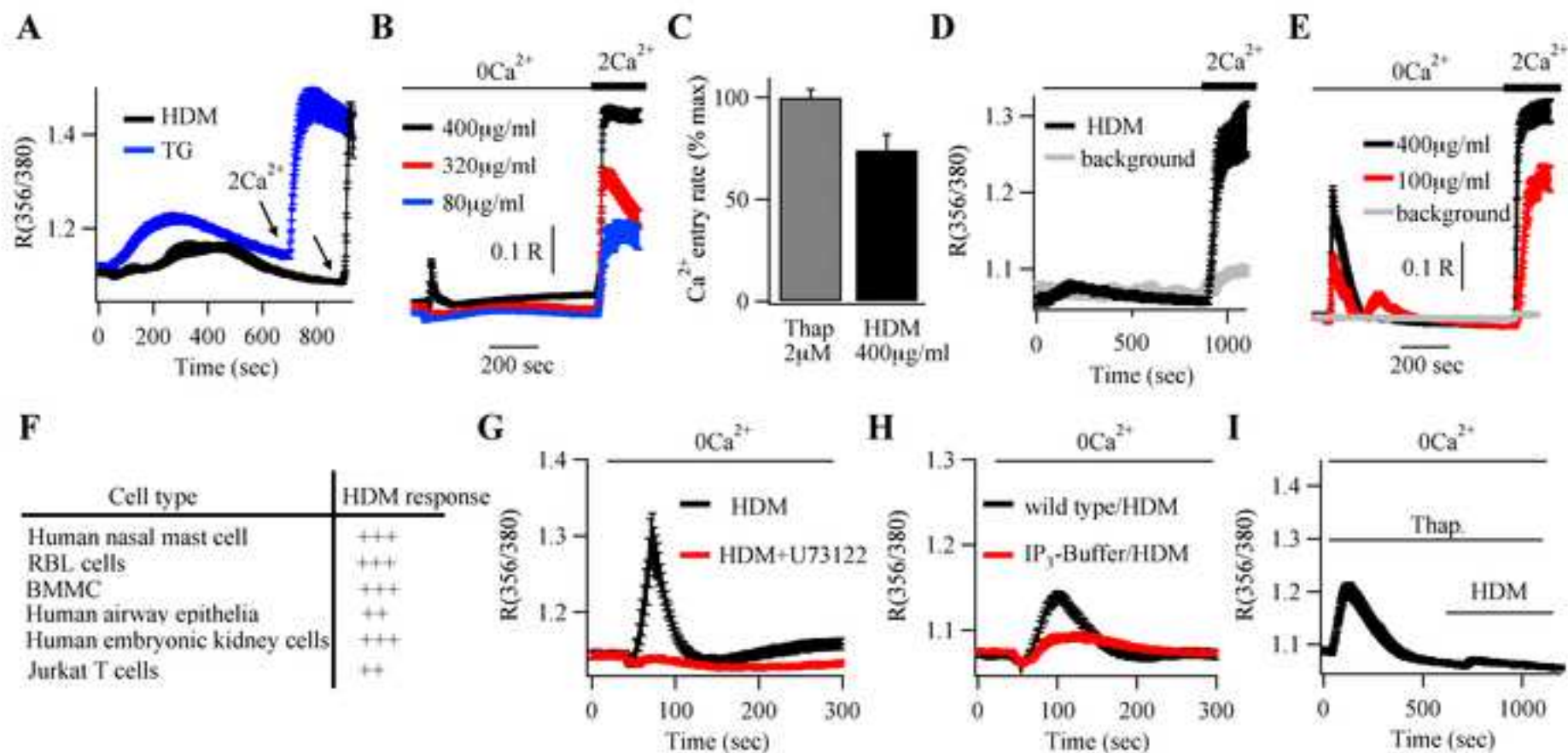
Data are presented as mean \pm SEM. Statistical significance was determined by using the Student's t test, except in Figures 2B, 2C, 4H, 5C, 7E and 7G, where ANOVA followed by a post hoc Newman-Keuls multiple comparison test was used (*p<0.05, **p<0.01).

Data and Software Availability

Raw images used in this study can be accessed using the Mendeley DOI link: <http://dx.doi.org/10.17632/46z5yp68dz.1>

Supplemental Information

Document S1; Table S1.



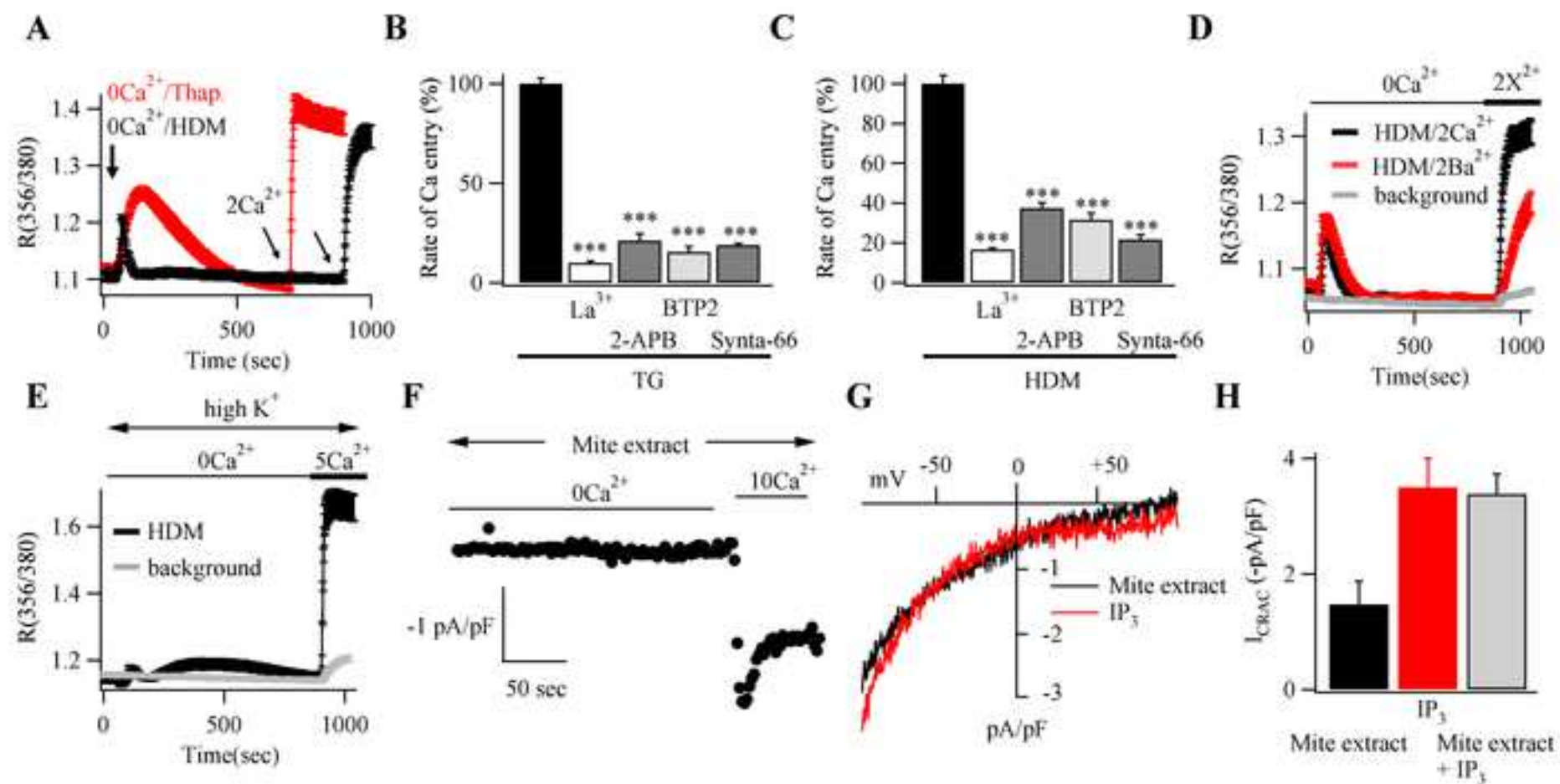
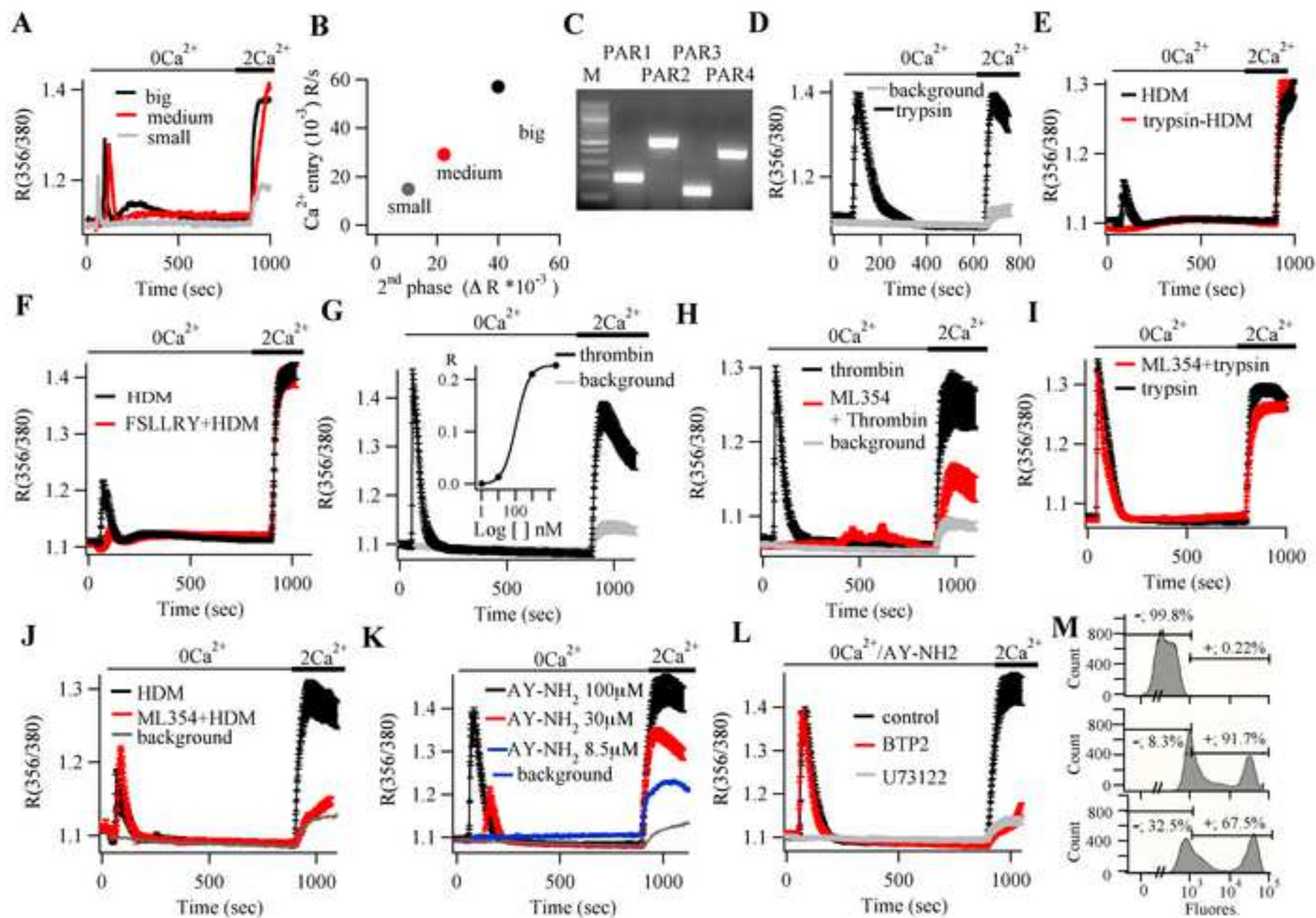
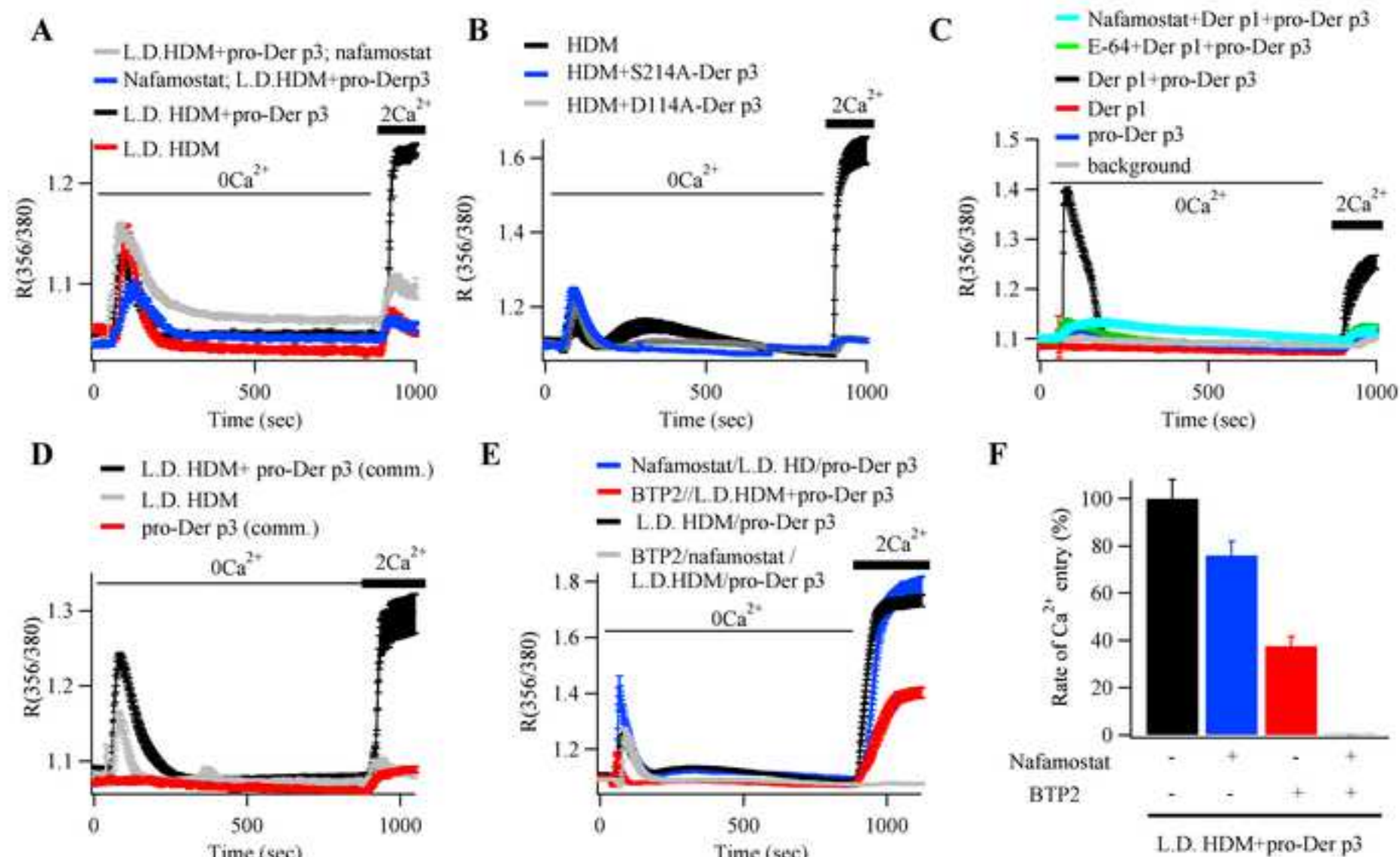
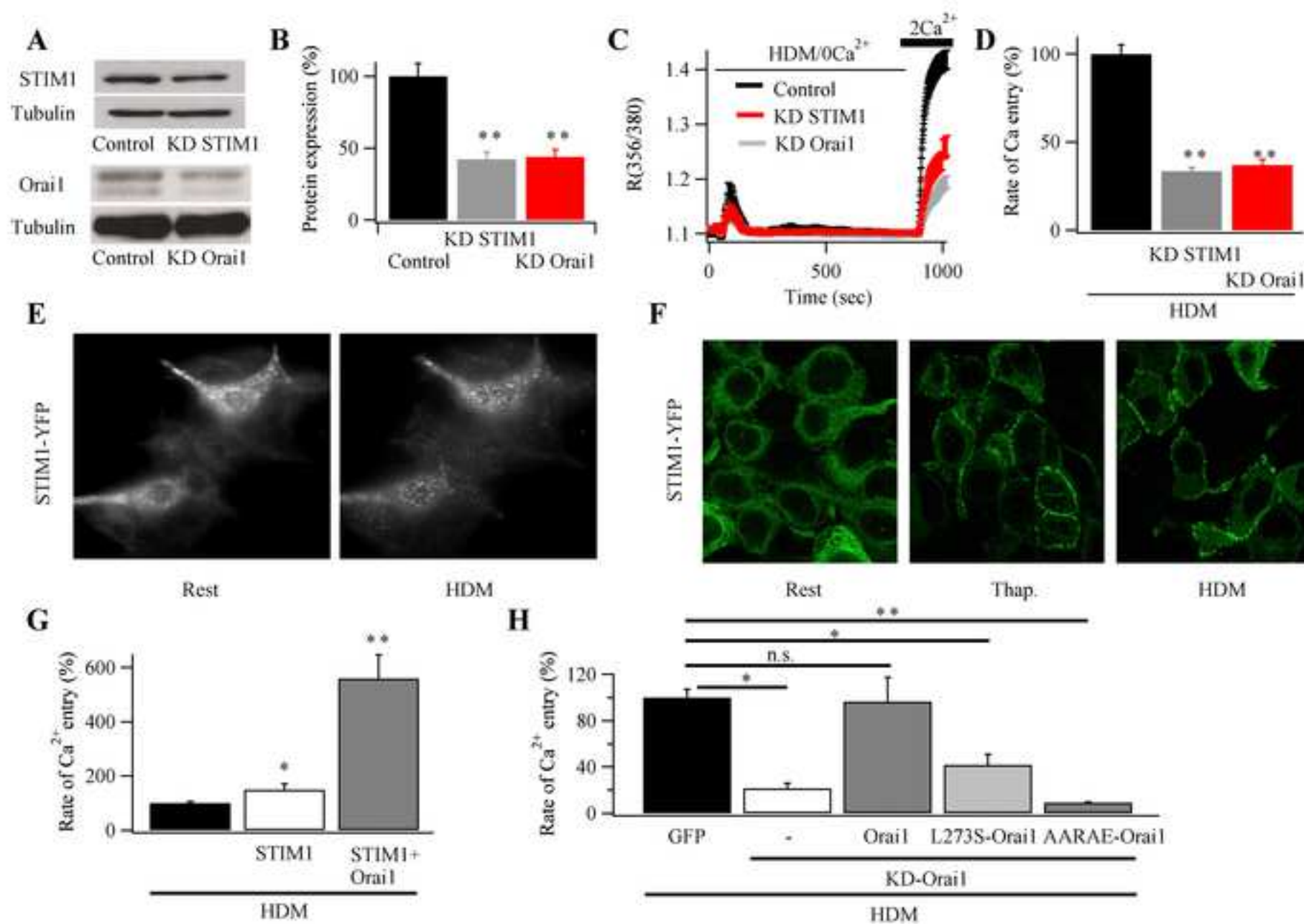
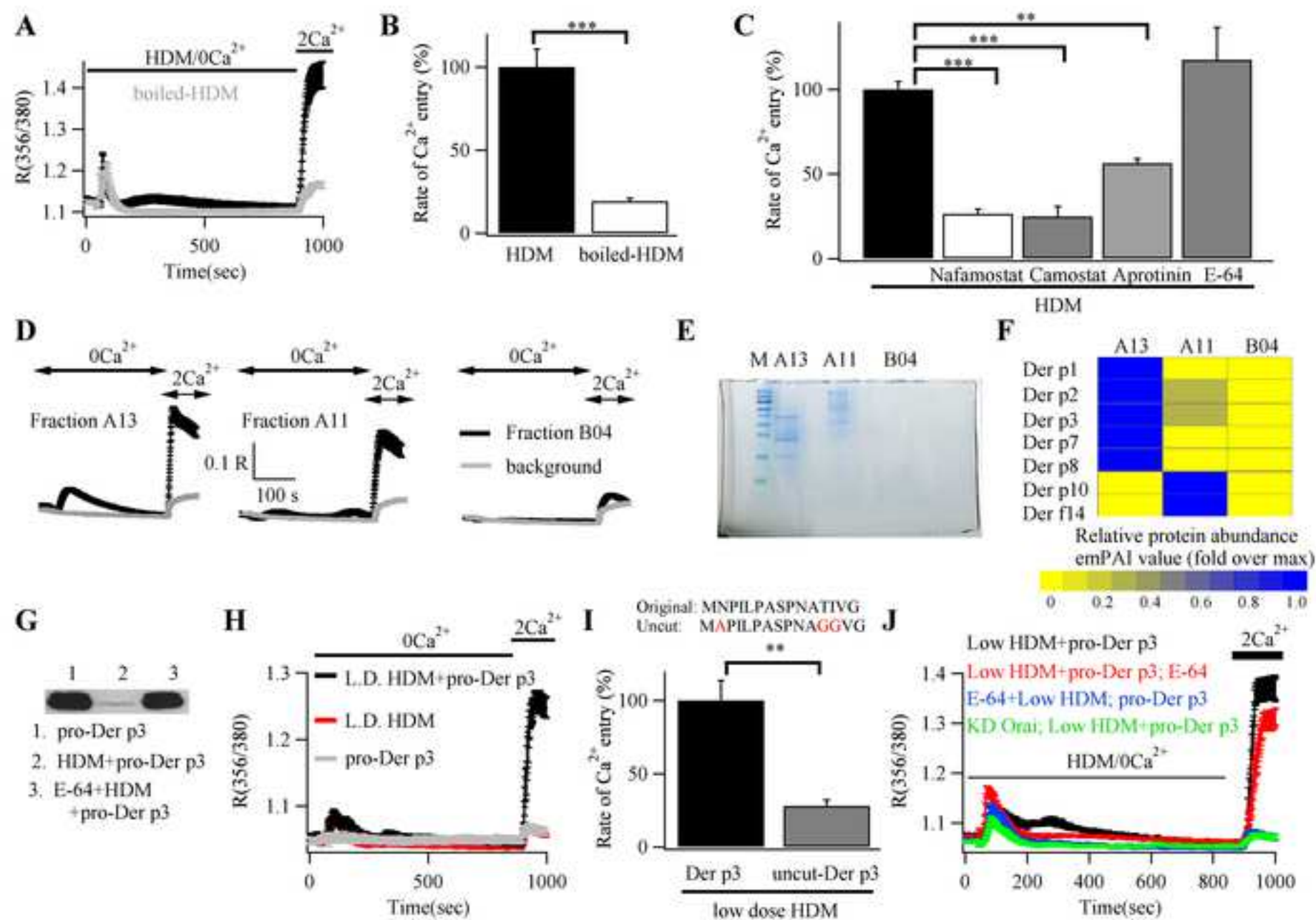


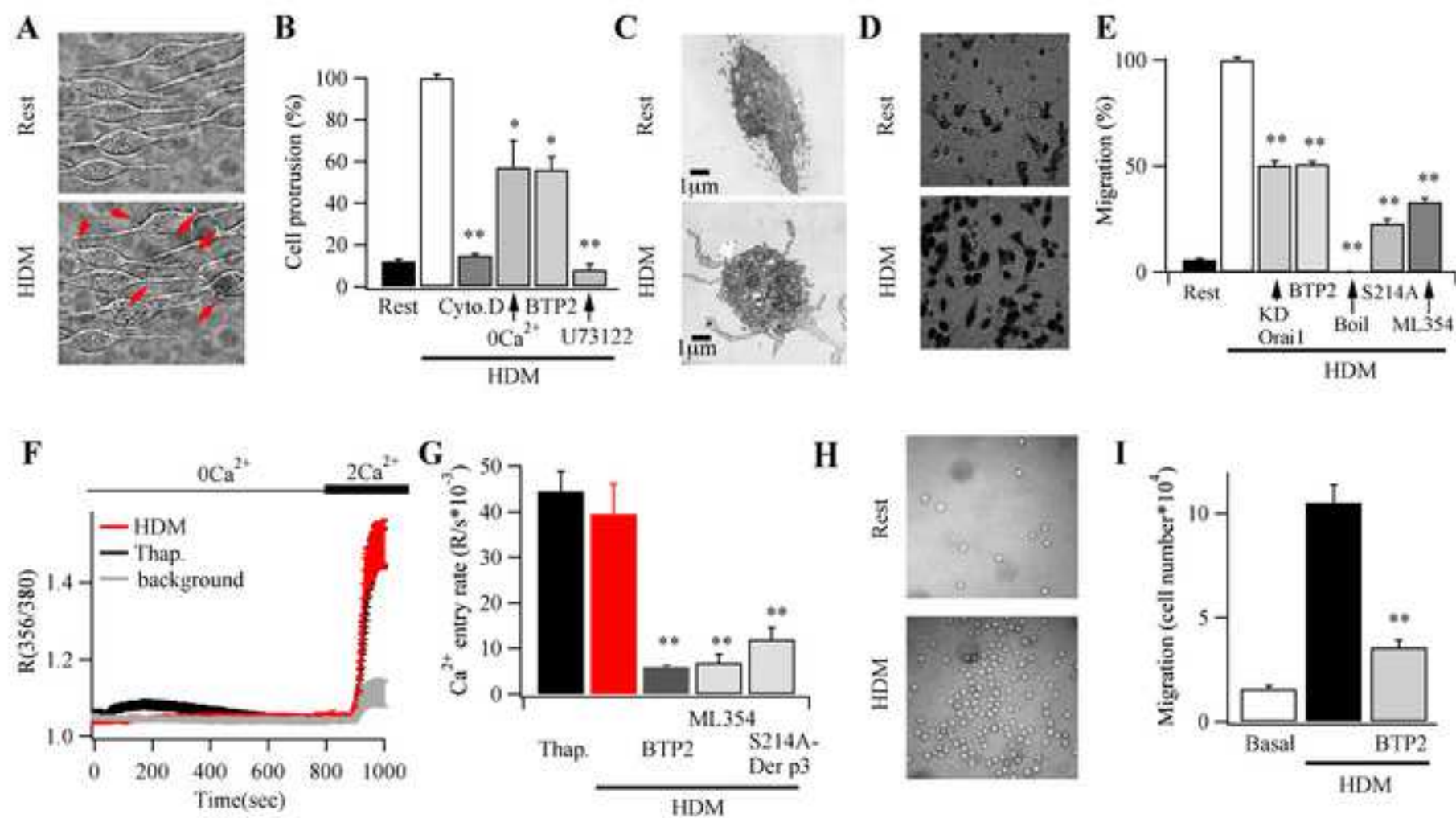
Figure3

[Click here to download Figure F3.tif](#)









Supplemental Information.

Supplemental Figure 1, related to Figure 1. Different lots of house dust mite extract elicit broadly similar rates of Ca^{2+} entry and do not affect fura 2 fluorescence. **A**, Comparison of different house dust mite extract lots on the rate of Ca^{2+} influx. Lots were bought over a four year period. Each point is the mean response (>15 cells) to mite extract applied at $400\ \mu\text{g}/\text{ml}$. Most lots had activity that differed less than 2-fold. Lot 262538 was more potent and the same lot, ordered at different times, gave responses that decreased in a time-dependent manner. The first lot of 262538 was not used for experiments. **B-C**, Background fluorescence of house dust mite extract. Although house dust mite extract has been used in several studies involving fluorescence measurements, we checked to see whether it exhibited any intrinsic fluorescence. RBL-2H3 cells (not loaded with fura 2) were excited at 356 and 380 nm excitation wavelengths and emission was collected $> 510\ \text{nm}$. No emission signal was detected at 356 or 380 nm excitation. After application of house dust mite in Ca^{2+} -free external solution, excitation at 356 nm and 380 nm both led to a small and stable increase in emission intensity, with the signal at 380 nm being slightly larger. The ratio (356/380) showed a very small decrease (panel B). Addition of 2 mM external Ca^{2+} led to small decreases in emission intensities following excitation at both 356 and 380 nm (380 nm excitation signal is shown in panel C). The ratio increased slightly (panel B). The fluorescent signals to mite extract have minimal effect on the Ca^{2+} signals we have recorded for the following reasons. First, the intensity changes at 356 and 380 nm excitation were tiny compared with those evoked by mite extract in fura 2-loaded cells (panels B and C). The ratio increase when Ca^{2+} was added to mite extract alone was 0.011 ± 0.007 whereas in fura 2 loaded cells it was 0.363 ± 0.053 . The decrease in emission following excitation at 380 nm was ~ 10 -fold larger in fura 2-loaded cells than with mite extract alone (panel C). Second, U73122 abolished the rise in the 356/380 ratio when mite extract was applied to fura 2-loaded cells, showing the vast majority of the Ca^{2+} signal emanated from intracellular Ca^{2+} release and not from the presence of mite extract itself (Figure 1G). Third, the large rise in the fura 2 ratio when Ca^{2+} was readmitted to fura 2 loaded cells activated by mite extract in Ca^{2+} -free solution was almost completely suppressed by block of the channels with BTP2 (Figure 2), or after knockdown of Orai1 (Figures 3B-C). Collectively, these results show that the small intrinsic fluorescence from mite extract has virtually no impact on the Ca^{2+} signals recorded with fura 2.

Supplemental Figure 2, related to Figure 3. Lack of correlation between the size of the first Ca^{2+} release transient and the extent of store-operated Ca^{2+} entry. **A**, The rate of Ca^{2+} entry is plotted against the amplitude of the first phase of Ca^{2+} release. The labels small, medium and large refer to the size of the second Ca^{2+} release phase which occurred after the first phase. For the point marked big, the second phase was big but the first phase was smaller in size than it was when the second phase was medium or small. The first phase was relatively large for those cells that showed a small second phase, but Ca^{2+} influx was less despite the larger initial Ca^{2+} release component. **B**, RT-PCR compares expression of PAR receptors in HEK293 cells.

Supplemental Figure 3, related to Figure 3. Effects of receptor desensitization and inhibitors on PAR-mediated Ca^{2+} signals. **A**, Desensitization of PAR2 receptors to the agonist trypsin. RBL-2H3 cells were exposed to trypsin (0.1 mg/ml) for 10 minutes in Ca^{2+} -free solution and then cells were perfused with Ca^{2+} -containing external solution without trypsin. After 15 minutes, trypsin was added again in Ca^{2+} -free solution (grey trace; labelled after trypsin pre-pulse). The recording was broken (indicated by slashed lines) to minimise bleaching of fura 2 during the interpulse interval. No Ca^{2+} release occurred. Readmission of external Ca^{2+} led to a small rise in cytosolic Ca^{2+} , which was similar in size to the background response obtained following perfusion with Ca^{2+} -free solution (without trypsin) for the same time. Control responses from cells not pre-treated with trypsin are shown. Control response denotes mean of 23 cells and after trypsin pre-pulse 31 cells. **B**, The PAR4 antagonist ML354 has no effect on thapsigargin-evoked Ca^{2+} release or subsequent store-operated Ca^{2+} entry. Thap trace denotes control cells (mean of 12 cells). ML354 denotes cells pre-treated with 3 μM ML354 for 15-20 minutes (mean of 11 cells).

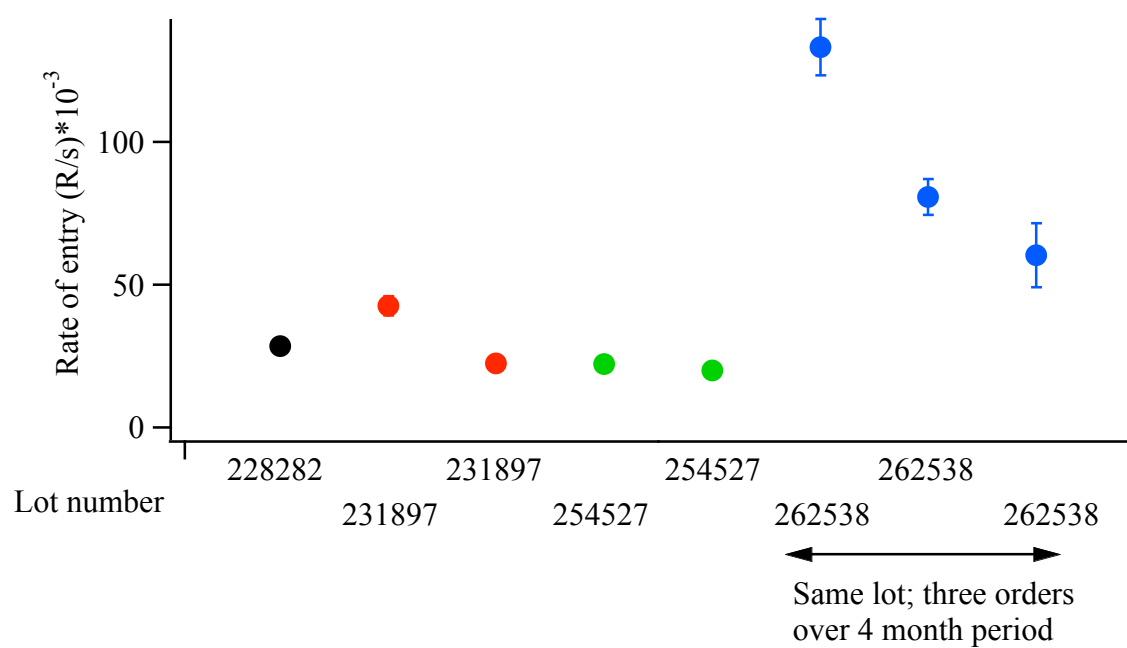
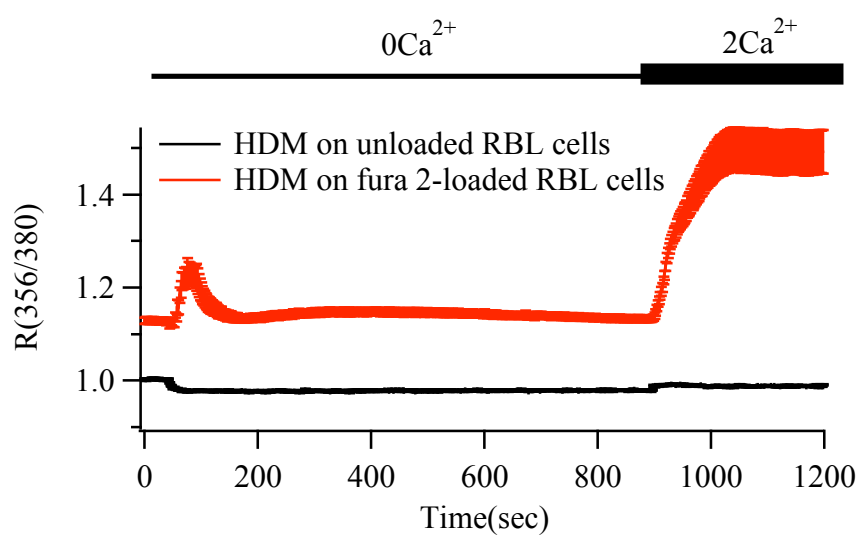
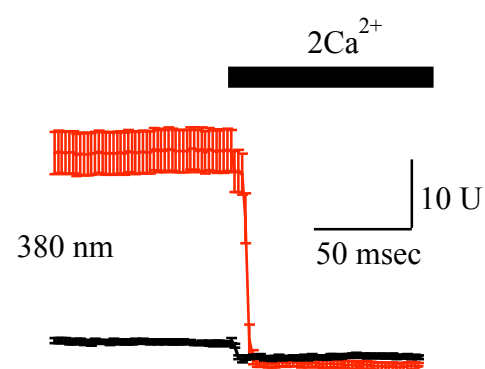
Supplemental Figure 4, related to Figure 5. Serine protease activity of Der p3 is required for Ca^{2+} entry. **A**, Nafamostat does not affect store-operated Ca^{2+} entry. RBL-2H3 cells were treated with thapsigargin in Ca^{2+} -free external solution and then external Ca^{2+} was readmitted. Cells were pre-treated with nafamostat for 15 minutes and the drug was present throughout the experiment. Control trace is the mean of 9 cells and nafamostat the mean of 10 cells. **B**, BTP2 inhibits Ca^{2+} influx activated by the combination of a low dose of house dust mite (HDM) and pro-Der p3. Each bar is the mean of between 14 and 22 cells. Cells were exposed to 10 μM BTP2 for 10 minutes before challenge. **C**, Catalytically inactive Der p3 fails to stimulate Ca^{2+} entry. Whereas exposure to a low dose (L.D.) of house dust mite and pro-Der p3 activates Ca^{2+} release and prominent Ca^{2+} entry, catalytic mutants of Derp3 (S214A-Der p3 and D114A-Der p3) are ineffective. A low dose of house dust mite without exogenous pro-der p3 failed to activate significant Ca^{2+} entry. L.D. HDM trace is the mean of 16 cells, L.D. HDM + pro-Der p3 19 cells, L.D. HDM + S214A-Der p3 30 cells and L.D. HDM + D114A-Der p3 24 cells. **D**, Boiling of commercial pro-Der p3 suppresses Ca^{2+} influx. Exposure to low dose house dust mite and pro-Der p3 results in robust store-operated Ca^{2+} influx (trace is mean of 14 cells). However, no Ca^{2+} influx occurred when pro-Der p3 was boiled (and then cooled) prior to mixing with house dust mite (trace is mean of 18 cells).

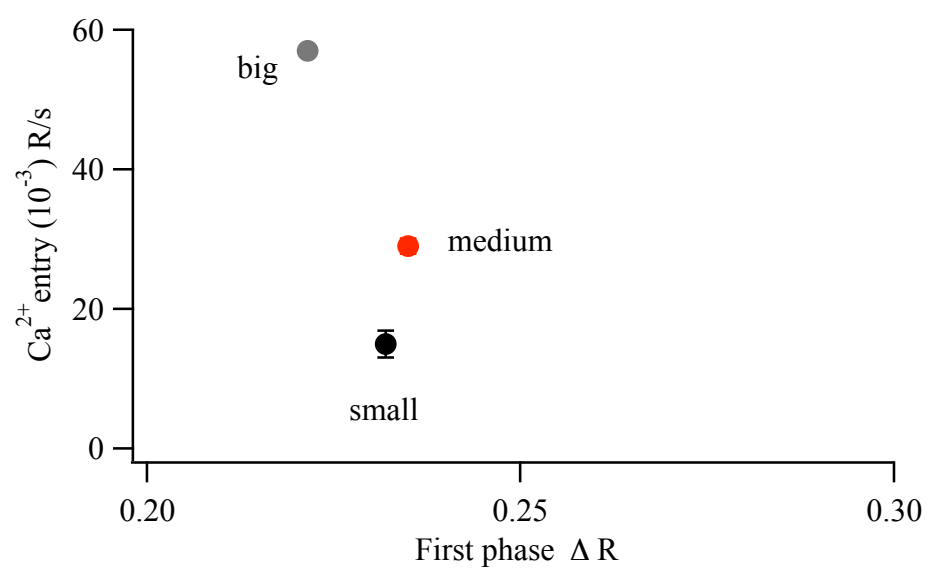
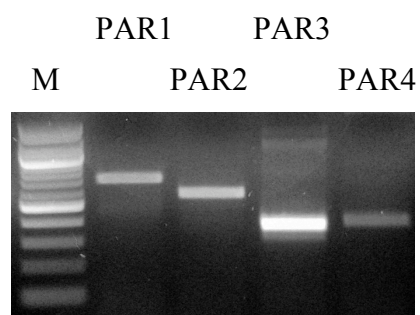
Supplemental Figure 5, related to Figure 5. Interaction between Der p1 and Der p3 regulates Ca^{2+} entry. **A**, Silver staining confirms purity of commercial Der p1 and commercial pro-Der p3. **B**, Ca^{2+} influx to the combination of Der p1 and pro-Der p3 is inhibited by BTP2 (10 μM ; 10 minutes pre-treatment). In these experiments, commercial Der p1 and recombinant his-tagged pro-Der p3 were used. Background is mean of 15 cells, Der p1 + pro-Der p3 is mean of 11 cells and BTP2+ Derp1 + pro-Der p3 is mean of 8 cells.

Supplemental Figure 6, related to Figure 5. Der p3 activates PAR4 receptors. **A**, Pre-treatment with a high dose of house dust mite extract reduces fluorescein-conjugated PAR4 peptide association with the cell membrane. **B**, PAR4 peptide

binding is significantly reduced by pre-exposure of RBL-2H3 cells to Der p3 but not by the S214A-Der p3 mutant that lacks catalytic activity. In these experiments, recombinant pro-Der p3 or pro-Der p3 mutant was mixed with a low dose of mite extract prior to addition to cells. Fluorescein-conjugated peptide was added 10 minutes later.

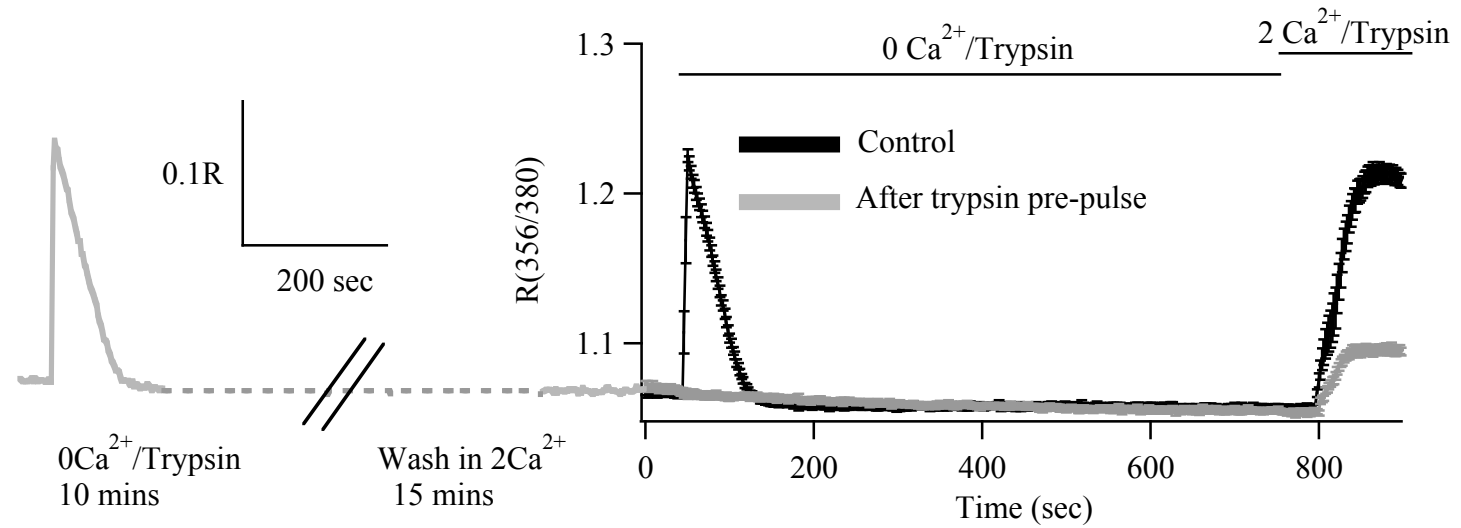
Supplemental Figure 7, related to Figures 5 and 6. Measurements of the catalytic activity of Der p3 and the various mutants used. **A**, Serine protease activity of the various proteins shown are compared. Uncut –Der p3 refers to pro-der p3 with mutations in the cleavage site (see Figure 5I for further details). **B**, The graph compares protease activity for different concentrations of trypsin. The X shows the corresponding activity of Der p3 used in our experiments, equating with 0.033 mg/ml trypsin. We used a well-established assay for serine protease activity to measure catalytic activity of Der p3 and the various mutants of Der p3 used in the preceding sections. Serine proteases cleave N_α -Benzoyl-L-arginine *p*-nitroanilide hydrochloride to release the chromophore *p*-nitroaniline, which can be detected by colorimetric analysis.

A**B****C**

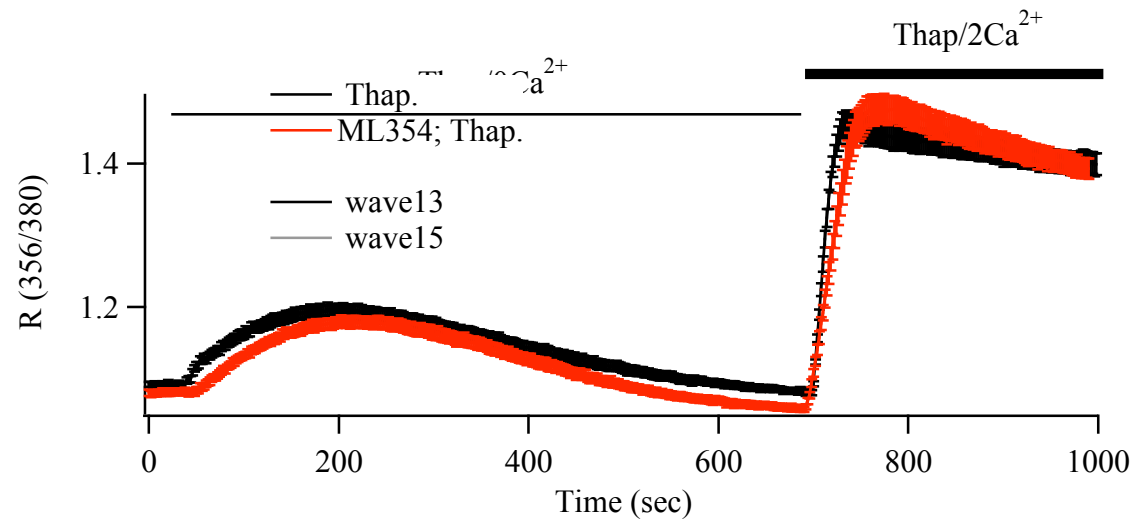
A**B**

Supplemental Figure 3

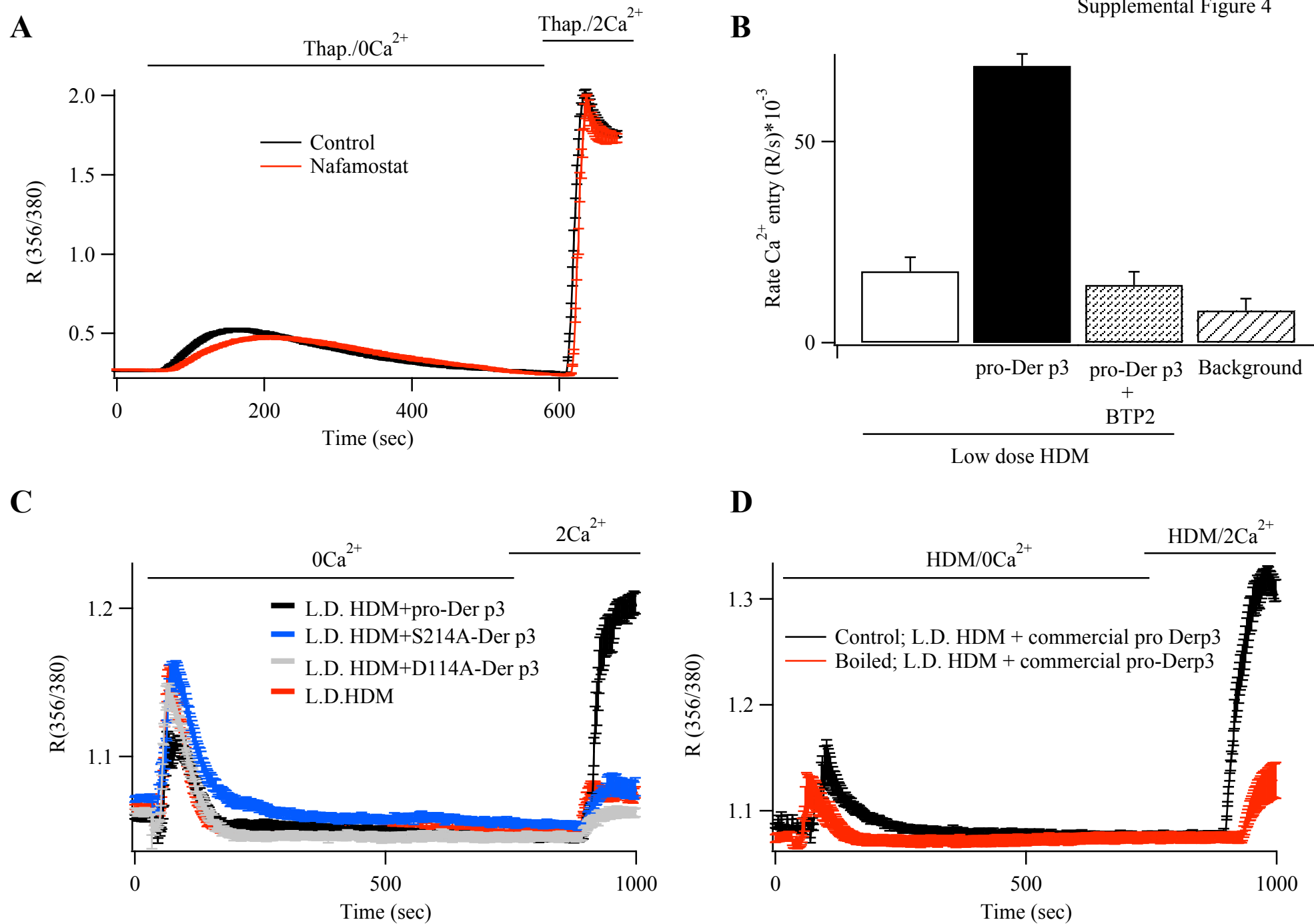
A

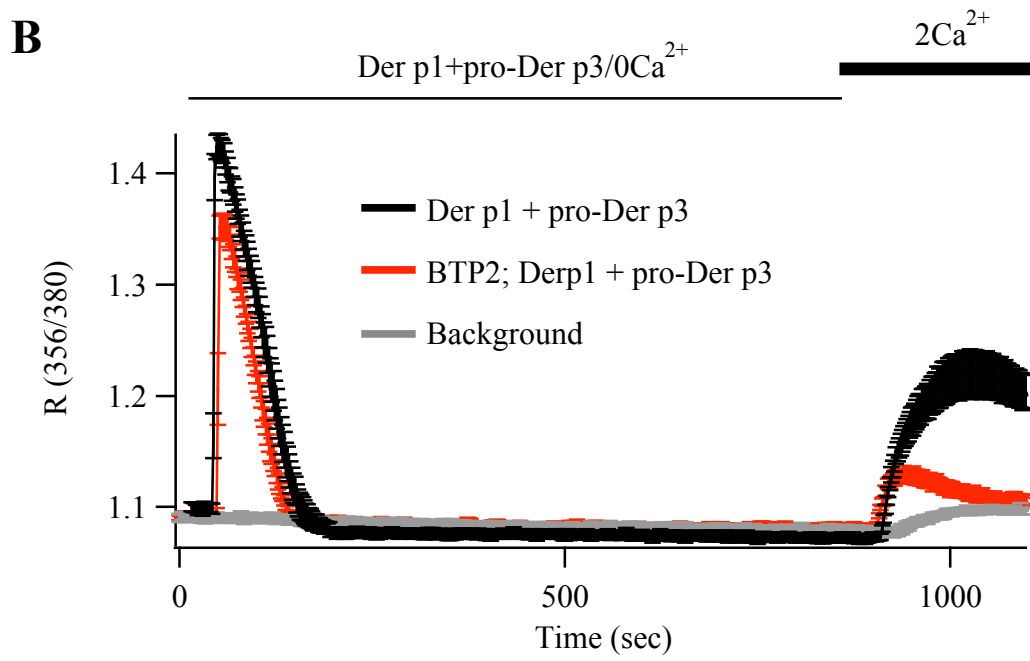
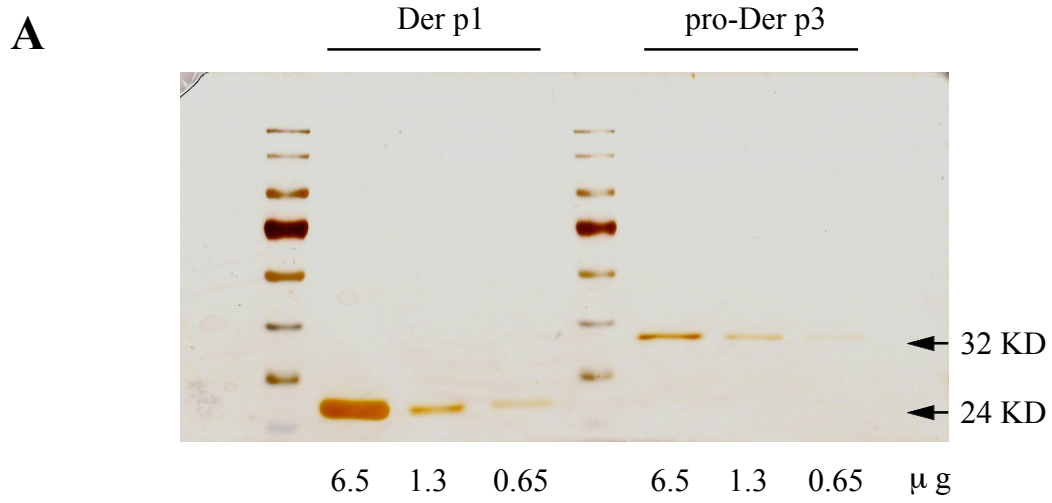


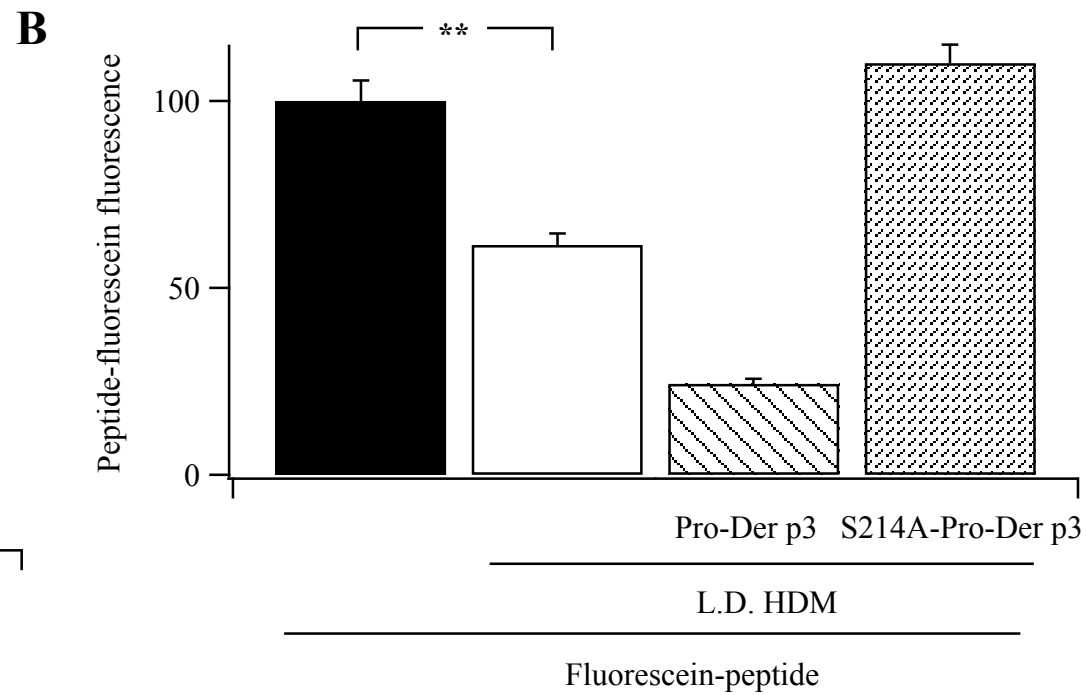
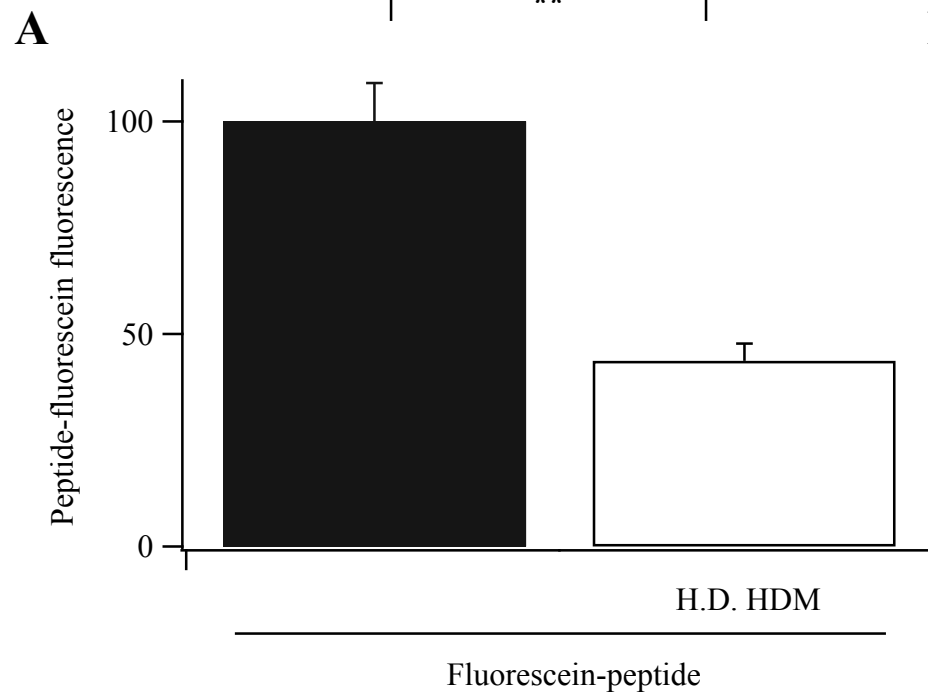
B



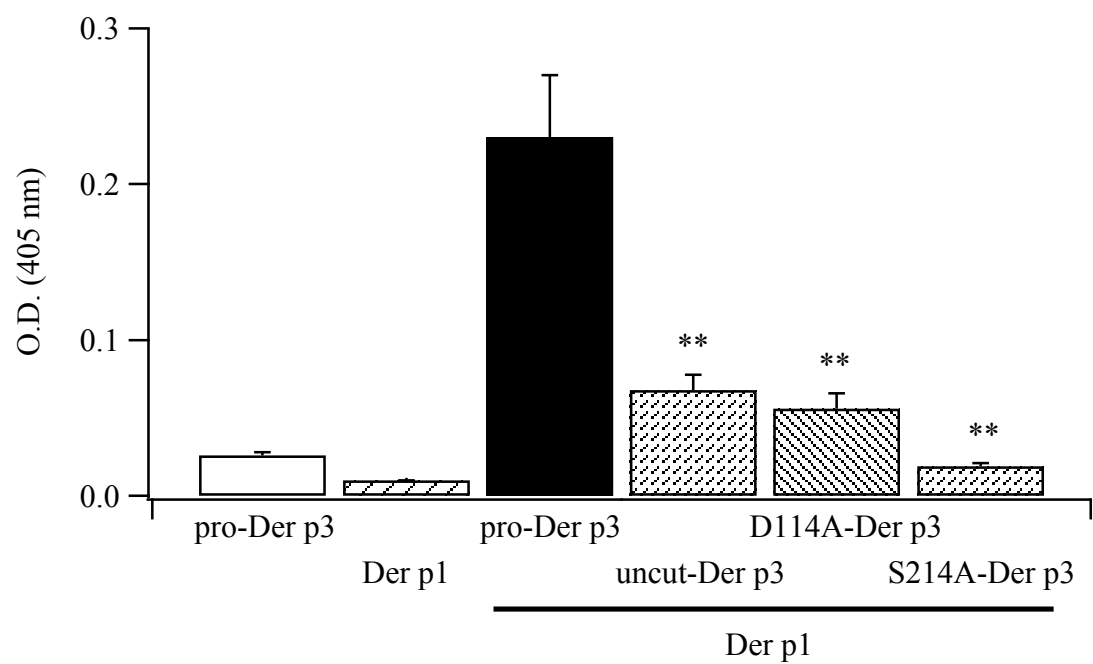
Supplemental Figure 4



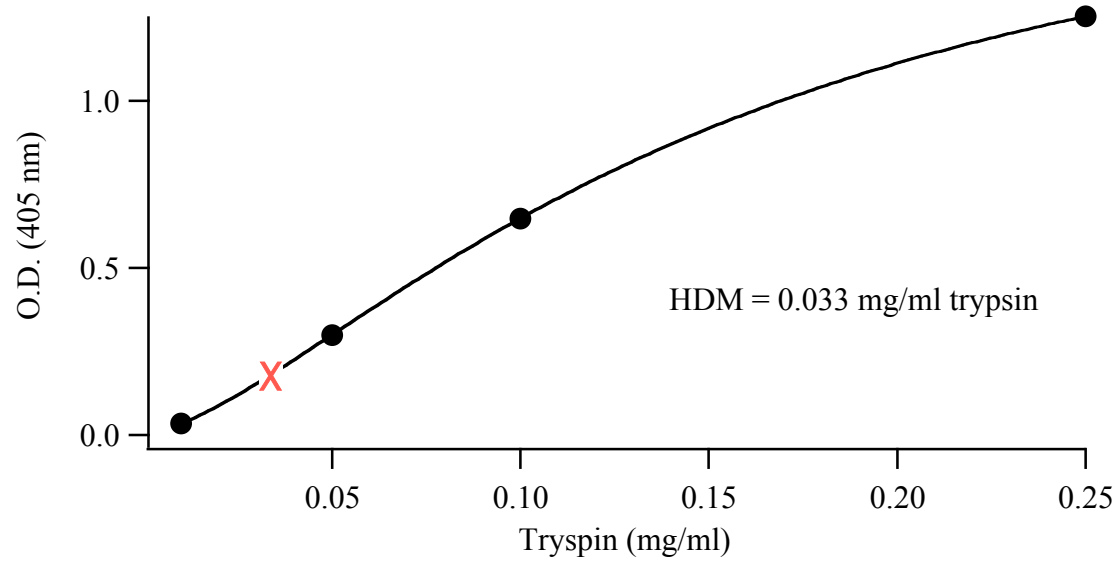




A



B



Accession	Score	Number of matches	Number of significant matches	Number of sequences	Number of significant sequences	Sequence coverage [%]	Description
O18416	417	107	28	48	14	82	Tropomyosin
P46419	113	39	6	19	4	69	Glutathione S-transferase
P49278	104	25	3	14	1	72	Mite group 2 allergen Der p 2
P39675	87	17	3	15	3	57	Mite allergen Der p 3
P49273	73	12	1	11	1	47	Mite allergen Der p 7
P39673	56	42	2	28	2	62	Allergen Mag (Fragment)
P08176	51	8	1	7	1	28	Peptidase 1 Der p 1

Supplemental Table 1, related to Figure 5. Protein hits assigned to *Dermatophagoides* species from MASCOT search of Uniprot_Swissprot database (taxonomy restriction: 'other metazoa'); significant protein hits displayed at 1% false discovery rate (FDR)

Accession	Score	Number of matches	Number of significant matches	Number of sequences	Number of significant sequences	Sequence coverage [%]	Description
gi 20385544	523	138	33	87	29	53	group 14 allergen protein
gi 60920912	308	48	10	14	4	51	glutathione transferase delta-like Dp7018E11
gi 60920899	243	38	9	16	6	65	glutathione transferase mu class Dp7002H05
gi 2353266	150	57	7	25	5	59	tropomyosin
gi 67975089	109	13	3	12	3	23	group 15 allergen protein short isoform
gi 386698135	83	11	3	8	2	16	heat shock protein cognate 5, partial
gi 15072346	82	4	1	4	1	23	ferritin heavy chain-like protein
gi 729315	75	4	1	4	1	20	Mite allergen Der p 3
gi 1352240	73	2	1	2	1	9	Mite allergen Der p 7
gi 1352237	71	11	2	5	1	51	Mite group 2 allergen Der p 2
gi 37958173	70	10	1	7	1	13	Der f Alt a 10 allergen
gi 60920878	69	18	3	9	3	45	glutathione transferase mu class Dp7019C10
gi 37958175	54	3	1	1	1	3	Der f Gal d 2 allergen
gi 83754032	51	4	1	4	1	30	Mature And Fully Active Der P 1 Allergen

Supplemental Table 1 related to Figure 5 continued. Protein hits assigned to *Dermatophagoides* species from MASCOT search of NCBI nr database (taxonomy restriction: 'other metazoa'); significant protein hits displayed at 1% false discovery rate (FDR)